Pergamon

Geochimica et Cosmochimica Acta, Vol. 59, No. 11, pp. 2345–2374, 1995

0016-7037/95 $9.50 + .00

0016-7037(95)00110-7

Cogenetic rock fragments from a lunar soil: Evidence of a ferroan noritic-anorthosite pluton on the Moon

B. L. JOLLIFF and L. A. HASKIN

Department of Earth and Planetary Sciences and the McDonnell Center for the Space Sciences, Washington University, St. Louis, MO 63130, USA

(*Received October* 6, 1994; *accepted in revised form March* 3, 1995)

Abstract—The impact that produced North Ray Crater, Apollo 16 landing site, exhumed rocks that include relatively mafic members of the lunar ferroan anorthositic suite. Bulk and mineral compositions indicate that a majority of 2–4 mm lithic fragments from sample 67513, including impact breccias and monomict igneous rocks, are related to a common noritic-anorthosite precursor. Compositions and geochemical trends of these lithic fragments and of related samples collected along the rim of North Ray Crater suggest that these rocks derived from a single igneous body. This body developed as an orthocumulate from a mixture of cumulus plagioclase and mafic intercumulus melt, after the plagioclase had separated from any cogenetic mafic minerals and had become concentrated into a crystal mush (~70 wt% plagioclase, 30 wt% intercumulus melt). We present a model for the crystallization of the igneous system wherein "system" is defined as cumulus plagioclase and intercumulus melt. The initial accumulation of plagioclase is analogous to the formation of thick anorthosites of the terrestrial Stillwater Complex; however, a second stage of formation is indicated, involving migration of the cumulus-plagioclase–intercumulus-melt system to a higher crustal level, analogous to the emplacement of terrestrial massif anorthosites. Compositional variations of the lithic fragments from sample 67513 are consistent with dominantly equilibrium crystallization of intercumulus melt. The highly calcic nature of orthocumulus pyroxene and plagioclase suggests some reaction between the intercumulus melt and cumulus plagioclase, perhaps facilitated by some recrystallization of cumulus plagioclase. Bulk compositions and mineral assemblages of individual rock fragments also require that most of the mafic minerals formed in close contact with cumulus plagioclase, not as separate layers. The distribution of compositions (and by inference, modes) has a narrow peak at anorthosite and a broader, larger peak at noritic anorthosite.

Characteristics of the samples and their geochemical trends imply an origin in a system that was large relative to the (unknown) size of the impact that produced the breccias of ferroan noritic-anorthosite composition that were excavated later by the formation of North Ray Crater, and they appear to be consistent with an origin of the suite within a perched plagioclase cumulate. If the Moon's crust formed by accumulation of plagioclase in a magma ocean, ferroan noritic anorthosite, formed as an orthocumulate, is an alternative to extensive adcumulus formation of ferroan anorthosite (>90 vol% plagioclase). This provides a relatively mafic ferroan anorthositic component (~15 vol% mafics), which is required by mass-balance models of compositions of polymict lunar-crustal materials. The inferred bulk composition of the system of cumulus plagioclase and intercumulus melt is similar to that of ferroan regolith breccia MacAlpine Hills 88104/5, a lunar-highland meteorite, and may represent a common and widespread component of the Moon's early highland crust.

"... current knowledge of structural relationships among lunar highland rocks is such that more conventional avenues of reasoning are not appropriate."

McCallum et al. (1975)

INTRODUCTION

That the Moon differentiated early and rapidly to form a crust and mantle is generally accepted, and the most popular model for this differentiation is solidification of a global magma ocean. In that scenario, dense mafic minerals produced the lunar mantle, and less dense plagioclase rafted to the surface or upper parts of the ocean to produce a ferroan, plagioclase-rich crust. Other proposed scenarios involve serial magmatism, i.e., repeated intrusion of many anorthosite-producing magmas into the upper crust (e.g., Walker, 1983; Longhi and Ashwal, 1985). Determining just how the early lunar differentiation processes operated will help us understand the early differentiation of other planets, including Earth.

The impossibility of field mapping of lunar plutonic formations and the extensive modification of accessible highland igneous rocks by meteoroid impact has complicated this task. We know little about relative abundances of different plutonic lithologies and petrogenetic relationships among them. Were there large bodies of nearly pure (>95%) plagioclase, implying an efficient and widespread adcumulus* process (e.g.,

* *Cumulus terminology.* We use cumulus terminology with the meanings ascribed by Wager et al. (1960) and reviewed more recently by Wadsworth (1985). *Cumulus* plagioclase refers to crystals that nucleated and grew from magma as primary crystals and were subsequently removed to a bounding surface where they accumulated, in this case, as a suspended or rafted layer. Initially, cumulus grains are partially enclosed by *intercumulus melt* or *liquid* having the composition of contemporary magma. Eventual solidification would lead to *intercumulus material*, which might take the form of overgrowths on cumulus grains, interstitial grains, or reaction with or replacement of cumulus grains. Any modifications subsequent to the initial accumulation phase are *postcumulus*, without regard to a specific process. *Adcumulates* form when intercumulus liquid is squeezed out by postcumulus growth of cumulus grains combined with selective diffusion, leading to further growth of cumulus grains of uniform composition. *Orthocumulates* form when intercumulus liquid solidifies in place, producing normally zoned rims on cumulus grains as well as interstitial grains of several minerals.

Table 1. Chemical compositions of selected 2–4 mm particles from sample 67513, Station 11.

sample # (67513,7xxx)		,7008 [1]Fragmental Bx	,7011 Bx + An Clast	,7012 Gabbronorite	,7024 Fragmental Bx	,7040 Impact-melt Bx	,7052 Anorthosite	,7061 Nor Anorthosite
mass (mg)		32.3	33.1	40.5	42.1	33.7	39.8	26.8
Major Elements (E - electron microprobe of fused beads, I - INAA, (mr) - modal recombination)								
SiO_2	(E)	45.2 ± 0.25	44.7 ± 0.17	48.0 ± 0.38	44.9 ± 0.24	44.9 ± 0.35	44.6 (mr)	45.4 ± 0.84
TiO_2	(E)	0.37 ± 0.07	0.09 ± 0.016	1.36 ± 0.05	0.27 ± 0.022	0.32 ± 0.044	0.03 (mr)	0.12 ± 0.07
Al_2O_3	(E)	27.8 ± 0.31	31.7 ± 0.21	11.1 ± 0.39	28.0 ± 0.14	29.5 ± 0.58	33.1 (mr)	30.2 ± 1.2
Cr_2O_3	(E)	0.11 ± 0.02	0.05 ± 0.025	0.39 ± 0.03	0.09 ± 0.03	0.10 ± 0.02	0.04 (mr)	0.07 ± 0.03
Cr_2O_3	(I)	0.107	0.045	0.398	0.108	0.080	0.045	0.074
FeO [1]	(E)	5.63 ± 0.15	3.01 ± 0.06	15.68 ± 0.34	6.02 ± 0.12	4.29 ± 0.13	1.66 (mr)	3.96 ± 0.37
FeO [1]	(I)	5.92 ± 0.08	2.82 ± 0.04	15.76 ± 0.22	6.17 ± 0.09	4.07 ± 0.06	1.65 ± 0.03	3.70 ± 0.05
MnO	(E)	0.11 ± 0.02	0.05 ± 0.02	0.24 ± 0.02	0.08 ± 0.02	0.06 ± 0.02	0.02 (mr)	0.06 ± 0.02
MgO	(E)	4.02 ± 0.09	1.78 ± 0.04	10.08 ± 0.15	3.48 ± 0.05	3.08 ± 0.14	1.59 (mr)	2.19 ± 0.22
CaO	(E)	16.74 ± 0.18	18.22 ± 0.10	12.93 ± 0.08	16.71 ± 0.09	17.32 ± 0.14	18.80 (mr)	17.63 ± 0.19
CaO	(I)	16.4 ± 0.8	18.3 ± 0.4	13.2 ± 0.5	16.7 ± 0.6	17.0 ± 0.4	18.3 ± 0.4	17.4 ± 0.4
Na_2O	(E)	0.31 ± 0.02	0.30 ± 0.01	0.19 ± 0.01	0.36 ± 0.01	0.39 ± 0.02	0.29 (mr)	0.40 ± 0.01
Na_2O	(I)	0.321 ± 0.005	0.328 ± 0.005	0.189 ± 0.003	0.372 ± 0.005	0.413 ± 0.006	0.274 ± 0.004	0.391 ± 0.006
K_2O	(E)	0.016 ± 0.007	0.014 ± 0.007	0.010 ± 0.008	0.020 ± 0.008	0.014 ± 0.007	0.01 (mr)	0.03 ± 0.01
P_2O_5	(E)	0.02 ± 0.04	<0.02 ± 0.02	0.03 ± 0.02	<0.02	0.03 ± 0.02		<0.02
Oxide Sum		100.6	99.7	100.1	100.2	99.8	99.7	99.8
Mg' [2]		0.56	0.51	0.53	0.51	0.56	0.63	0.50
Trace Elements (INAA)								
Sc		13.6 ± 0.2	6.3 ± 0.1	42.4 ± 0.6	13.2 ± 0.2	9.8 ± 0.2	3.20 ± 0.05	10.1 ± 0.2
Cr		730 ± 10	308 ± 4	2720 ± 40	740 ± 10	549 ± 8	307 ± 4	503 ± 7
Co		8.3 ± 0.1	2.31 ± 0.03	15.7 ± 0.2	7.1 ± 0.1	5.3 ± 0.1	1.72 ± 0.02	1.86 ± 0.03
Ni		<19	<53	<51	n.d.	<38	<14	<35
Zn		20 ± 1	n.d.	52 ± 7	n.d.	n.d.	5.2 ± 0.6	n.d.
Rb		1.4 ± 0.5	<1.8	<7	0.9	<2	<1.6	<2
Sr		149 ± 7	147 ± 9	70 ± 17	121 ± 13	158 ± 11	145 ± 7	157 ± 11
Zr		19 ± 6	<29	85 ± 24	24 ± 12	28 ± 11	<16	<47
Cs		0.070 ± 0.009	0.045 ± 0.015	<0.16	<0.09	0.039 ± 0.017	0.022 ± 0.009	0.05 ± 0.03
Ba		20 ± 6	22 ± 3	<45	<39	22 ± 4	10 ± 3	14 ± 4
La		1.34 ± 0.03	0.573 ± 0.010	2.81 ± 0.05	1.143 ± 0.025	1.61 ± 0.025	0.17 ± 0.006	0.496 ± 0.014
Ce		3.84 ± 0.12	1.57 ± 0.08	7.4 ± 0.6	3.02 ± 0.17	4.53 ± 0.13	0.45 ± 0.05	1.30 ± 0.08
Nd		<4	<4	7.3 ± 2.2	<4	3.2 ± 0.9	n.d.	<6
Sm		0.781 ± 0.015	0.310 ± 0.004	1.85 ± 0.03	0.654 ± 0.012	0.906 ± 0.014	0.078 ± 0.002	0.276 ± 0.004
Eu		0.752 ± 0.011	0.733 ± 0.013	0.530 ± 0.012	0.706 ± 0.013	0.843 ± 0.014	0.661 ± 0.012	0.843 ± 0.016
Tb		0.194 ± 0.005	0.075 ± 0.006	0.490 ± 0.018	0.152 ± 0.008	0.206 ± 0.008	0.018 ± 0.003	0.077 ± 0.007
Yb		0.834 ± 0.024	0.336 ± 0.009	2.04 ± 0.04	0.728 ± 0.024	0.809 ± 0.017	0.074 ± 0.005	0.368 ± 0.011
Lu		0.124 ± 0.007	0.048 ± 0.002	0.290 ± 0.008	0.101 ± 0.005	0.117 ± 0.003	0.010 ± 0.001	0.055 ± 0.002
Hf		0.60 ± 0.017	0.148 ± 0.016	1.75 ± 0.05	0.47 ± 0.03	0.65 ± 0.022	0.044 ± 0.01	0.179 ± 0.019
Ta		0.067 ± 0.005	0.02 ± 0.01	0.286 ± 0.016	0.069 ± 0.009	0.088 ± 0.008	<0.016	<0.06
Ir		0.7 ± 0.3	<0.9	<2	<6	0.9 ± 0.4	<0.5	<1.6
Au		<1.9	<1.2	<4	<2	<0.13	<0.7	<1.6
Th		0.142 ± 0.012	0.057 ± 0.010	0.41 ± 0.03	0.144 ± 0.017	0.187 ± 0.012	0.018 ± 0.005	0.036 ± 0.009
U		<0.2	<0.1	<0.3	<0.18	<0.16	<0.05	<0.14

Oxide concentrations given in weight percent; trace elements in ppm; Au and Ir in ppb. Oxide sum includes Cr_2O_3, FeO, and Na_2O as determined by INAA and other oxides as determined from analysis of fused beads or modal recombination. [1]Total Fe reported as FeO. [2]Mg' calculated using FeO (E). "n.d." - not detected. Uncertainties are 1-σ estimates of analytical precision. [1]Sample descriptions: ,7008 - complex fragmental breccia; ,7011 - glassy-matrix breccia with coarse anorthositic clast; ,7012 - relict-igneous gabbronorite; ,7024 - complex crystalline/fragmental-matrix breccia; ,7040 - clast-bearing impact-melt breccia; ,7052 - igneous, anorthosite; ,7061 - relict-igneous noritic anorthosite.

Ryder, 1992), or did ferroan anorthosite form small masses within rock bodies that were overall more mafic? Did some ferroan anorthositic rocks form mainly by orthocumulus processes or by rafting of small portions of cumulus mafic minerals, making them somewhat more mafic than typical ferroan anorthositic rocks in the Apollo samples (e.g., Warren, 1990)? Was there crude layering of early crustal differentiates, with plagioclase-rich anorthosites accumulating preferentially at some level (e.g., Hawke et al., 1992)?

The most direct information has come from identification and characterization of surviving fragments of plutonic rocks that retain igneous texture (see Warren, 1993, summary of "pristine" highland rocks). Such rocks, however, make up only a small fraction of returned highland samples. Most returned highland materials are polymict soils and breccias that derive from a broader variety of igneous rocks than the larger plutonic fragments represent. We need to learn how to determine the identities, relative abundances, and modes of origin of their parent lithologies. In this paper, we show how a suite of mostly polymict lithic fragments collected from the rim of North Ray Crater may represent a large plutonic body and, if so, what constraints they provide on the nature of geochemical processes that produced their igneous precursor.

PREVIOUS WORK

Rocks of the ferroan anorthositic suite are abundant among the North Ray Crater samples, both as monomict igneous rocks and as clasts in polymict breccias. Many are ferroan anorthosite (sensu stricto, i.e., >90 vol% plagioclase), but more mafic rocks that have similar mineral compositions are also common and occur mainly as clasts in feldspathic breccias such as 67015 (Marvin et al., 1987), 67016 (Norman, 1981; Norman et al., 1991; Norman and Taylor, 1992), 67035 (Ryder and Norman, 1979), 67075 (Hubbard et al.,

Table 1. Continued.

sample # (67513,7xxx) mass (mg)	,7071 †Anorthosite 24.6	,7075 Anorthosite 16.2	,7088 Complex Breccia 27.6	,7097 Gabbronorite 18.2	AN-G Anorthosite 43.6	BHVO-1 Basalt 11.0
Major Elements (E - electron microprobe of fused beads, I - INAA, (mr) - modal recombination)						
SiO_2 (E)	44.3 (mr)	44.1 (mr)	46.8 ± 0.67	47.6 ± 0.79		
TiO_2 (E)	0.02 (mr)	0.01 (mr)	0.28 ± 0.04	0.34 ± 0.11		
Al_2O_3 (E)	35.8 (mr)	34.7 (mr)	23.6 ± 0.83	20.0 ± 1.1		
Cr_2O_3 (E)	0.001 (mr)	0.01 (mr)	0.12 ± 0.02	0.22 ± 0.02		
Cr_2O_3 (I)	0.001	0.013	0.131	0.202		
FeO † (E)	0.20 (mr)	0.90 (mr)	8.20 ± 0.49	10.48 ± 0.35		
FeO † (I)	0.204 ± 0.003	0.87 ± 0.01	8.14 ± 0.12	10.81 ± 0.15	2.95 ± 0.04	11.09 ± 0.16
MnO (E)	0.001 (mr)	0.02 (mr)	0.12 ± 0.03	0.16 ± 0.02		
MgO (E)	0.16 (mr)	0.62 (mr)	5.27 ± 0.38	6.67 ± 0.27		
CaO (E)	19.66 (mr)	19.35 (mr)	15.13 ± 0.26	14.19 ± 0.04		
CaO (I)	18.9 ± 0.4	18.0 ± 0.7	15.4 ± 0.6	14.5 ± 0.3	15.8* ± 0.4	11.2 ± 0.9
Na_2O (E)	0.37 (mr)	0.30 (mr)	0.27 ± 0.02	0.24 ± 0.01		
Na_2O (I)	0.372 ± 0.005	0.276 ± 0.004	0.276 ± 0.004	0.244 ± 0.003	1.66* ± 0.02	2.27 ± 0.03
K_2O (E)	0.01 (mr)	0.01 (mr)	0.02 ± 0.01	0.04 ± 0.01		
P_2O_5 (E)	<0.01 (mr)	<0.02 (mr)	0.02 ± 0.02	<0.02 ± 0.02		
Oxide Sum	100.4	100.0	99.8	100.3		
Mg'	0.58	0.55	0.53	0.53		
Trace Elements (INAA)						
Sc	0.33 ± 0.005	1.5 ± 0.022	16.1 ± 0.23	26.2 ± 0.4	10.0 ± 0.14	31.0 ± 0.4
Cr	10.5 ± 0.15	88 ± 1.2	898 ± 13	1379 ± 19	47.6 ± 0.7	291 ± 4
Co	0.11 ± 0.003	0.3 ± 0.007	13.2 ± 0.19	14.1 ± 0.2	24.6 ± 0.3	45.1 ± 0.6
Ni	3.3 ± 1.3	n.d.	<27	<56	40 ± 11	132 ± 20
Zn	1.41 ± 0.14	2 ± 0.4	18 ± 1.1	28 ± 1.7	22.5 ± 1.2	118 ± 3
Rb	0.48 ± 0.11	1.1 ± 0.3	2.1 ± 0.7	<6	<3	11.2 ± 2.2
Sr	164 ± 3	155 ± 7	134 ± 9	108 ± 15	81 ± 10	397 ± 21
Zr	<10	<10	25 ± 8	<80	<39	185 ± 22
Cs	0.041 ± 0.003	0.096 ± 0.008	0.041 ± 0.013	0.10 ± 0.05	0.046 ± 0.018	0.10 ± 0.03
Ba	8.4 ± 0.8	8 ± 3	15 ± 7	28 ± 8	38 ± 5	117 ± 15
La	0.123 ± 0.004	0.226 ± 0.015	1.27 ± 0.03	2.19 ± 0.03	2.22 ± 0.05	15.5 ± 0.23
Ce	0.273 ± 0.016	0.58 ± 0.05	3.44 ± 0.11	6.09 ± 0.2	4.92 ± 0.10	37.7 ± 0.6
Nd	0.36 ± 0.16	n.d.	<6	5.7 ± 1.6	3.0 ± 1.4	21 ± 3
Sm	0.048 ± 0.002	0.099 ± 0.003	0.718 ± 0.012	1.351 ± 0.019	0.742 ± 0.012	6.2 ± 0.1
Eu	0.771 ± 0.011	0.718 ± 0.012	0.727 ± 0.013	0.695 ± 0.015	0.361 ± 0.009	2.04 ± 0.04
Tb	0.007 ± 0.001	0.02 ± 0.003	0.172 ± 0.006	0.334 ± 0.012	0.179 ± 0.007	0.95 ± 0.02
Yb	0.027 ± 0.002	0.103 ± 0.012	0.789 ± 0.024	1.42 ± 0.03	0.84 ± 0.02	2.00 ± 0.06
Lu	0.0019 ± 0.0003	0.018 ± 0.003	0.124 ± 0.007	0.203 ± 0.005	0.118 ± 0.004	0.282 ± 0.018
Hf	0.0078 ± 0.0025	0.044 ± 0.009	0.51 ± 0.018	0.69 ± 0.03	0.41 ± 0.02	4.6 ± 0.09
Ta	<0.005	<0.03	0.052 ± 0.009	0.065 ± 0.018	0.16 ± 0.01	1.2 ± 0.03
Ir	<0.3	<0.7	<1.9	<6	<2	<3
Au	<1.4	<1.7	<2	<3	<4	<7
Th	<0.007	0.020 ± 0.005	0.129 ± 0.011	0.264 ± 0.022	0.048 ± 0.007	1.19 ± 0.04
U	<0.13	<0.1	<0.2	<0.17	<0.20	0.46 ± 0.17

See caption to first half of table. †Total Fe reported as FeO. ‡Sample descriptions: ,7071 - igneous, anorthosite; ,7075- cataclastic anorthositic breccia; ,7088 - complex crystalline -fragmental-matrix breccia; ,7097 - relict-igneous gabbronorite. *AN-G used as analytical standard for CaO & Na_2O.

1974; McCallum et al., 1975), 67215 (Lindstrom and Salpas, 1983; McGee, 1987; Warren et al., 1990), 67455 (Ryder and Norman, 1979), and 67975 (McGee, 1987; James et al., 1987). Warren (1990, 1993) has compiled lists and characteristics of specific rocks and clasts.

Much previous work has been done to relate the various members of the ferroan anorthositic suite of rocks to each other petrogenetically. James et al. (1989) define four subgroups of ferroan anorthosites based on mineral compositions and modes—mafic-magnesian, mafic-ferroan, anorthositic-sodic, and anorthositic-ferroan subgroups. James et al. (1989, 1991) concluded that there was no adequate petrogenetic scheme for the derivation of the entire ferroan anorthositic suite of rocks from a single magma. Recently, McGee (1993, 1994) has argued, on the basis of consistent compositional trends in plagioclase and pyroxene in all of the ferroan anorthosites, that the subgroups may have a common parental magma, but that secondary processes such as magma mixing, complex postcumulus history, disruption of the magmatic system, or postcrystallization shock metamorphism from impacts have imposed additional compositional variations.

ANALYTICAL METHODS

Sample Handling

Each of 219 2–4 mm lithic fragments from sample 67513 was rinsed ultrasonically and examined under a binocular microscope. Individual particles were weighed and sealed into ultrapure silica tubing for neutron irradiation. Following instrumental neutron activation analysis (INAA) and 12 months "cool-down" time, thirty-six particles that represent the compositional groups and endmembers indicated by INAA were selected for detailed study. These were sawn in two; one half was made into a polished thin section for petrographic analysis, and the other half was reserved for a fused bead. We made fused beads of twenty samples for major-element analysis.

Instrumental Neutron Activation Analysis

The individual 2–4 mm fragments were irradiated for times ranging from 24 to 48 h at a thermal neutron flux of 4.0×10^{13} n cm^{-2} s^{-1}. Samples and synthetic glass standards were radioassayed one

week following the irradiation and again two weeks later; each sample received a total of three or four radioassays during these periods. INAA methods are described in detail by Korotev (1991). Data reduction was done using the TEABAGS program (Lindstrom and Korotev, 1982). Estimates of analytical precision (1-σ) are given in Table 1. As a check on accuracy, we include in Table 1 analyses of standard rock powders AN-G anorthosite (Govindaraju and Roelandts, 1993) and BHVO-1 basalt (Gladney and Roelandts, 1988).

Fused Beads

Sample splits for fused beads, typically weighing 10–20 mg, were ground with an alumina mortar and pestle under acetone. Powders were fused on a Mo-strip resistance heater (Brown, 1977) under Ar at atmospheric pressure.

Electron Microprobe Analysis

Mineral compositions and bulk compositions of glasses, fine-grained breccia matrices, and fused beads were determined with a JEOL 733 electron microprobe, using different combinations of mineral, oxide, and glass standards, an accelerating voltage of 15 kV, and 20–40 nA beam currents, depending on the mineralogy of the target. Data were reduced by the method of Bence and Albee (1968). Analyses of breccia matrices, glasses, fused beads, and bulk exsolved pyroxenes were done with a broad beam (30–50 μm). A minimum of five analyses was done on each fused bead. The analytical precision of this technique is limited by the homogeneity of the target; spot-to-spot standard deviations (one-σ, $n-1$) are shown in Table 1. Terrestrial basaltic glass standards were used as controls for the fused-bead and matrix analyses. For breccia matrices, which consist of glass and mineral phases of different density, we report concentration ranges that incorporate corrections assuming density variations involving anorthite and low-Ca pyroxene (see Albee et al., 1977, and Nazarov et al., 1982, for discussion of broad-beam analyses of multiphase targets).

DATA SET

Compositional Groups within Sample 67513

The 2–4 mm fragments from sample 67513 can be separated into two groups, mainly on the basis of compositional trends for incompatible and ferromagnesian trace elements, e.g., Sm and Sc (Fig. 1a). Incompatible trace elements (ITE) have relatively constant interelement ratios in many of the samples, so Sm concentrations are a good measure of the level of ITE enrichment. We select Sm because we determine its concentration very precisely by INAA. Scandium, also determined very precisely by INAA, is compatible in pyroxene, so its concentration is a measure of how mafic the sample assemblages are; samples with low Sc concentrations are rich in plagioclase and those with high Sc concentrations are rich in pyroxene.

The majority of the 67513 fragments (148 of 219; 70% by mass) have low ITE concentrations (<2 ppm Sm), Sc concentrations ranging from <1 ppm (equivalent to >95% plagioclase) to 42.4 ppm (equivalent to ~70% pyroxene), and high Sc/Sm values (>12, mean 17.6), typical of the ferroan anorthositic suite (Norman and Ryder, 1980). A good correlation between Sm and Sc concentrations extends to high Sc concentrations at low ITE concentrations and, from comparison with an extensive compilation of literature data, is more pronounced than in any other group of analyzed lunar samples (Fig. 1b). We include in this group all samples lying along or below the correlation line that extends from low Sm and low Sc concentrations to high Sc concentrations. Major-element data from electron-microprobe analysis of fused beads and from modal recombination, and trace-element data from INAA are given in Table 1 for a representative subset. This group is the main subject of this paper.

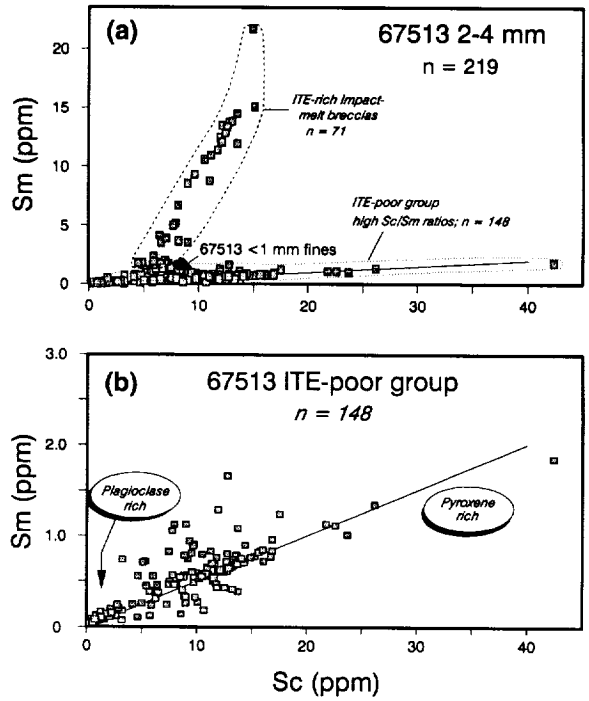

FIG. 1. (a) Concentrations of Sc vs. Sm for 2–4 mm lithic fragments from sample 67513. Two trends are evident: one extends to high Sc concentrations at low incompatible-trace-element (ITE) concentrations and the other extends to high ITE concentrations along the approximate trend of other impact-melt breccia groups from Apollo 16 (Korotev, 1994). The ITE-poor group shown in (b) with an expanded Sm scale is characterized by high Sc/Sm values that are typical of ferroan anorthositic-suite samples in general (the parameters of the line, by linear regression of all 148 lithic fragments, are an R^2 value of 0.68, a slope of 0.047 ± 0.003, and an intercept of 0.1 ± 0.2, effectively zero). The ITE-rich group includes impact-melt breccias that are unrelated, or of unknown relationship, to the ITE-poor group.

The second group comprises samples enriched in incompatible trace elements at relatively constant to slightly increasing Sc concentrations. These lithic fragments correspond compositionally to melt breccias of groups 2NR, 3, and 4 of Korotev (1994). They are not considered further in this paper.

The relationship of Sc concentrations to major-element compositions and mineral modes is illustrated on a plot of Sc vs. Al_2O_3 (Fig. 2). The ITE-poor igneous fragments from sample 67513 and other ferroan samples from North Ray Crater define a linear correlation extending from high Al_2O_3 and low Sc concentrations to low Al_2O_3 and high Sc concentrations. The Al_2O_3 concentrations of these samples range from those of anorthosite sensu stricto through gabbroic and noritic anorthosite to gabbronorite. The main reason for the correlation is different proportions of plagioclase (high Al, low Sc) and pyroxene (low Al, high Sc). Small variations in plagioclase or pyroxene compositions do not alter the correlation

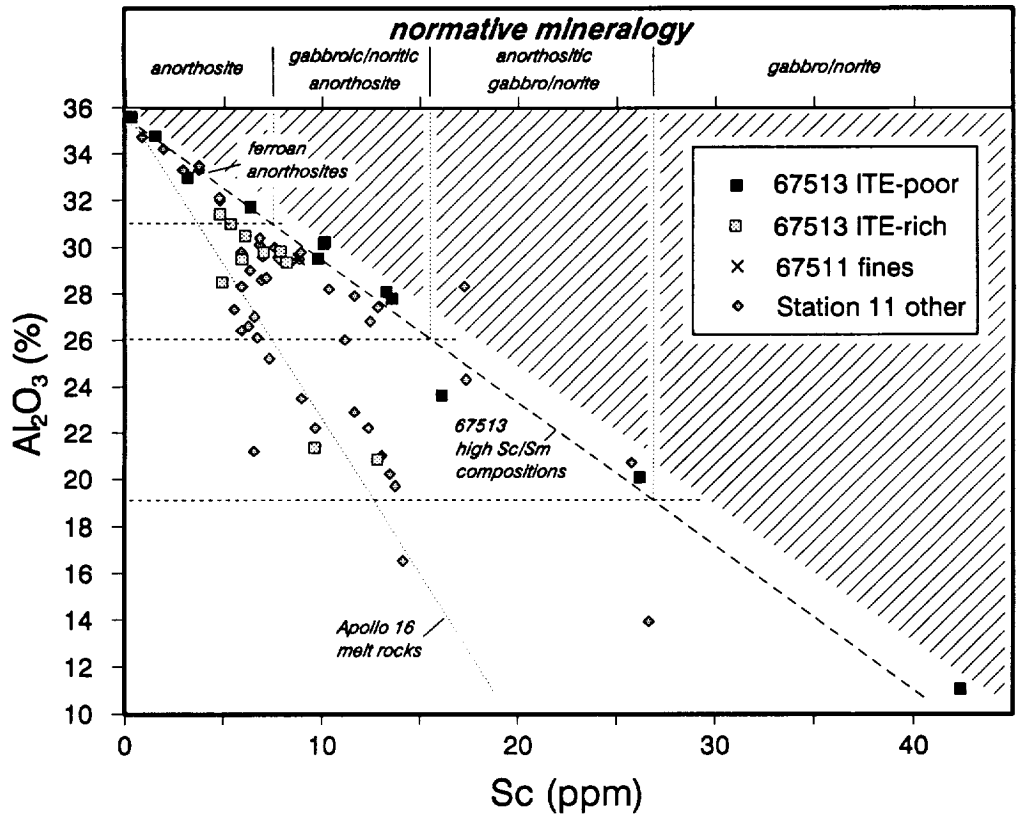

FIG. 2. Concentrations of Sc vs. alumina for lithic fragments from 67513 and other compositionally similar samples from North Ray Crater. Fields indicating normative mineralogy are based on alumina concentrations of assemblages according to the mineral proportions of Stöffler et al. (1980). The intersection of lines indicating alumina concentrations of field boundaries with the alumina-Sc correlation line for the ITE-poor group of particles from 67513 (solid squares) delineates the range of Sc concentrations for each indicated rock type for rocks of the ITE-poor group. "Station 11 other" refers to analyzed samples from Station 11 taken from the literature. The dotted line represents the approximate trend of compositions of impact-melt rocks from the Apollo 16 site (after Fig. 1, Korotev, 1994).

noticeably. Olivine, which could upset this correlation, is not modally abundant, i.e., generally ≤2%.

Lithology

Most of the 2–4 mm particles are fragmental breccias, impact-melt breccias, or combinations of the two types. Particles that have relict igneous or granulitic textures are subordinate. Many of the polymict particles, however, including fragmental and impact-melt breccias, contain recognizable lithic and mineral clasts of the same lithologies as the monomict, relict igneous samples. The Appendix contains descriptions of samples that represent the monomict lithologies.

Mineral compositions place the monomict samples in the ferroan anorthositic suite. Plagioclases range from ~An_{98} in some coarse grains to An_{93} in rims of relatively coarse grains in intercumulus assemblages and An_{90} in fine-grained interstitial plagioclase in those assemblages. Some plagioclase grains show minor compositional zoning (e.g., 2 An units). Plagioclase grains range up to several mm in size and range in form from blocky subhedral laths to large anhedral grains. Mafic silicates, dominantly pyroxenes, have Mg′ values [molar Mg/(Mg + Fe)] ranging from ~0.7–0.5 in pyroxenes (Table A3) and ~0.38–0.50 in olivine (Table A5); Mg′ values in monomict fragments are very uniform (e.g., Fig. 3). Pyroxenes are exsolved, but exsolution lamellae are generally thin (<20 μm). In samples containing subcalcic augite and calcic pigeonite grains, exsolution textures are complex, similar to those observed in 67075 (McCallum et al., 1975). In individual grains, lamellar components are homogeneous and compositions suggest intracrystalline diffusion and equilibration to ~800°C or less (Fig. 3). In several samples, inverted pigeonite overgrowths occur on rounded, subcalcic augite cores, and crystallization temperatures inferred from their compositions (Fig. 3a) suggest more than one episode of crystallization. Minor olivine occurs in several of the igneous lithic fragments. Concentrations of CaO are low (0.06–0.10), typical of plutonic origins, in olivine grains large enough to be unaffected by fluorescence from adjacent plagioclase or pyroxenes during electron-microprobe analysis (plutonic olivine generally <0.15% CaO; Ryder, 1992). Most of the igneous lithic fragments and clasts contain trace quantities of Cr-spinel ($Chr_{59-66}Ple_{20-28}Ulv_{8-18}$). Ilmenite is rare and is found only in the pyroxene-rich assemblages. Monomict lithic fragments range in mode from >99% anorthite to nearly 70% pyrox-

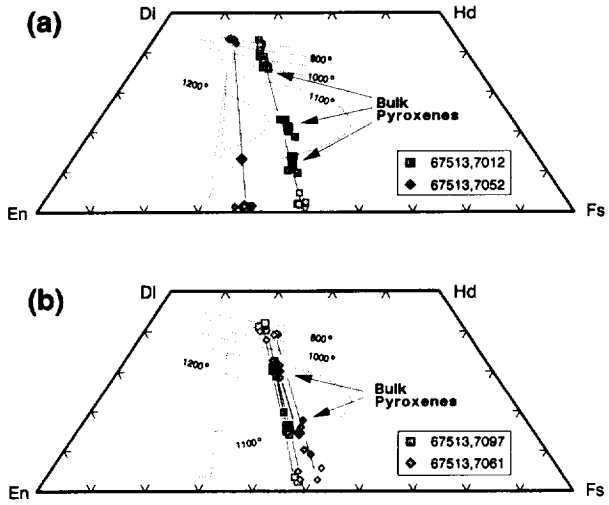

FIG. 3. Pyroxene quadrilateral compositions with isotherms superimposed from the two-pyroxene thermometer (low pressure) and "others" calculation method of Lindsley and Andersen (1983), temperatures in degrees centigrade. Dark-fill, large symbols are bulk pyroxene averages; medium-fill symbols are for individual broad-beam analyses of bulk pyroxenes; and light-fill, small symbols are for individual exsolved lamellae. (a) Composition plots for 67513,7012 gabbronoritic fragment and 67513,7052 anorthositic fragment. (b) Composition plots for 67513,7097 gabbronoritic fragment and 67513,7061 noritic-anorthosite fragment.

ene. We attach no special significance to the modes of individual lithic fragments; although we assign rock names, we view them as descriptions of assemblages and do not imply that any individual fragment is necessarily a modally representative sample of a larger rock.

Common among the ITE-poor lithic fragments in sample 67513 are polymict breccias that have ferroan igneous assemblages (i.e., low Mg′ mafic silicates and coexisting anorthitic plagioclase, mainly $\geq An_{95}$) as dominant clast components. We use the term "polymict" in the sense that they consist of a mixture of rock types, including meteoritic contamination. These polymict lithic fragments have bulk trace-element and major-element compositions, however, that are very similar to those of the monomict, igneous samples and that are diagnostic of their dominantly ferroan-suite assemblages, e.g., high Sc/Sm and Sc/Al_2O_3 values. The breccias also have low concentrations of siderophile elements; the mean Ni and Co concentrations of the ITE-poor fragments are 9 ppm and 6 ppm (Table 2), corresponding to less than 0.1% meteoritic contamination. The fine-grained fragmental matrices and melt matrices of the polymict breccias are sufficiently similar in composition to the clast lithologies that they do not cause the particle bulk compositions to differ much from what we expect for a mixture of their igneous clast components. Several representative breccias are described in the Appendix and their bulk compositions are given in Table 1.

DISCUSSION

The Monomict and Polymict Lithic Fragments as Samples of a Single Formation

On the basis of similar mineral assemblages, mineral compositions, bulk compositions, and compositional trends, we surmise that the lithic fragments, both monomict and polymict, are related petrogenetically to each other. The polymict breccias have low siderophile-element and incompatible-element concentrations, indicating little meteoritic contamination and an absence of KREEP-like components, and their clasts have ferroan-suite mineral assemblages. Melt and fragmental-matrix materials have essentially the same composition as the clasts; apparently, both derive from the same rocks. Despite the absence of absolute chemical pristinity and the paucity of well-preserved igneous textures, we believe these breccias stem from a common precursor; i.e., they are dominantly genomict, consisting mostly of petrogenetically related components (see Warren, 1993). Polymict fragments span the same compositional range as the monomict fragments with relict-igneous textures; thus, we suggest that the precursor to all was a single igneous rock body. McCallum et al. (1975) reached a similar conclusion regarding the "polymict" components of lunar rock sample 67075.

On the basis of geochemical characteristics such as high Sc/Sm and CaO/FeO values, and low Sm/Yb values, the igneous fragments and related breccias in sample 67513 may be interpreted as a ferroan, relatively mafic component of Descartes material (Stöffler et al., 1981; Jolliff, 1991). As such, they were probably excavated originally by the Nectaris basin impact (Stöffler et al., 1981). Petrographically, they are similar to clasts in breccias 67455 (Minkin et al., 1977; Lindstrom and Salpas, 1981, 1983), 67075 (McCallum et al., 1975), and 67215 (McGee, 1987). It is likely that the set of 67513 lithic fragments and those large breccias derive from a common precursor. We refer to the precursor igneous system that produced the fragments as the ferroan noritic-anorthosite (FNA) composition igneous system.

A Petrologic Model of the Precursor Igneous System

We offer three observations pertinent to determining the nature of the igneous system that was the precursor to these fragments. First, abundant breccias that are dominantly genomict offer a sampling advantage that complements information based on scarce monomict rocks. The genomict breccia fragments are a crudely averaged sample of some larger rock body. Such a body could be part of a pluton or a magma ocean.

Second, simple crystallization of a cotectic liquid would produce a much lower proportion of plagioclase relative to mafic minerals than we infer for the precursor igneous system. We thus take as a hypothesis that the precursor system was a mixture of plagioclase and cotectic melt. As we argue below, the incompatible-element concentrations of the mafic component are too high for it to be simply cumulus pyroxene. On the olivine-anorthite-silica pseudoternary projection, the compositions of these samples lie along a band between plagioclase and the plagioclase-olivine cotectic (Fig. 4a). From the position of the average composition of the fragments on the olivine-silica-anorthite pseudoternary projection, we calculate by mass balance a 70:30 mass ratio of plagioclase to cotectic material (Fig. 4b). Positive correlations between Sc and plagioclase-incompatible elements, such as trivalent REEs, and negative correlations between Sc and plagioclase-compatible

elements such as CaO and Al_2O_3, suggest that these rocks are, to a first approximation, mixtures of cumulus plagioclase (Sc-poor) and intercumulus melt (Sc-rich). The 70:30 relative proportions of "excess" plagioclase to cotectic melt is a value found for some terrestrial plagioclase cumulates (e.g., Haskin and Salpas, 1992) and corresponds to proportions of crystals at which magma-system viscosity rises sharply (Marsh and Maxey, 1985).

Third, the range of compositions of impact-melt and fragmental-matrix breccias suggests that, on a gross scale, feldspathic and mafic components of their precursor rocks were mixed, not widely separated. Bulk-breccia and melt-matrix compositions suggest that precursor rocks ranged from 23–31 wt% Al_2O_3, i.e., from anorthositic norite to gabbroic or noritic anorthosite. Impact melts (as inferred from breccia matrix) as feldspathic as anorthosite (>90 vol% plagioclase) or as mafic as norite or gabbro (<60 vol% plagioclase) are not found, suggesting that large segregations or layers of norite or gabbro were not present. We consider further the distribution of mafic and anorthositic rocks in the precursor in a later section.

Compositions of Cumulus Plagioclase, Intercumulus Melt, and the Bulk System

Compositions of ~75% of the 148 lithic fragments lie closely along the Sc-Sm correlation line of Fig. 1. These were used to determine regression lines such as those shown in Figs. 5 and 6 for all well correlated elements. From the mean Sc concentration of the lithic fragments (8.6 ppm) and the regression lines shown in Fig. 7, we obtain average concentrations for major elements not analyzed by INAA. The average composition, determined in this way, is approximately that of noritic anorthosite, with some 30 wt% Al_2O_3, 8.6 ppm Sc, and 0.5 ppm Sm (Table 2). The composition is ferroan, with bulk Mg′ of 0.56 and molar CaO/Al_2O_3 of 0.58, higher than that of anorthite (0.53–0.55). Concentrations of incompatible elements are very low, the trivalent REE are relatively unfractionated at 2–3 times chondritic values, and there is a positive Eu anomaly (Fig. 8). We refer to this average composition as the FNA igneous-system bulk composition.

We note that trace-element concentrations of the proposed system are similar to those of 67455 and are ~0.25–0.5 times those of Antarctic lunar meteorite MAC88104/5 (Table 2). The bulk system composition, expressed as a volume norm (85% plagioclase, 13% pyroxene, and 2% olivine), resembles the average mode of the Stillwater Middle Banded Zone (82% plagioclase, 15% pyroxene, and 2% olivine; McCallum et al., 1980). According to its normative mineralogy, low-Ca pyroxene exceeds high-Ca pyroxene by the ratio 7.6:5.1; thus, we refer to the system as noritic anorthosite rather than gabbroic anorthosite.

For geochemical modeling, we take the trace-element concentrations of cumulus plagioclase to be the average composition of the most plagioclase-rich samples analyzed by INAA that have low REE^{3+} concentrations. We take the plagioclase Fe and Mg concentrations to be those of relatively high Fe and Mg concentrations found with the electron microprobe in some regions of plagioclase-rich samples. These Fe and Mg concentrations are consistent with values obtained from samples retaining igneous textures by extrapolation of Fe and Mg concentrations vs. Sc concentrations to zero Sc concentration. For Na_2O and Eu, we take an average composition of the most plagioclase-rich samples (thirty-four lithic fragments). The resulting average cumulus plagioclase composition is given in Table 2.

We obtain the intercumulus (cotectic) melt composition by subtracting 70% of the average cumulus plagioclase composition from the FNA igneous-system bulk composition (Table 2, Col. 7) and dividing by 0.30. The Sc concentration of this melt is 28.1 ppm. The melt composition is sensitive only to the assumption that the system consists of cumulus plagioclase and cotectic melt, and is independent of whether the calculated system bulk composition is truly representative. The bulk composition merely indicates the relative proportions of cumulus plagioclase and melt of cotectic composition in the particular sampling of the rock body that the fragments constitute, whether the proportions are exactly that of the parent body or not.

We have defined the intercumulus melt as cotectic; we note that its composition, as calculated from mass balance, is what we would expect for a lunar ferroan melt. The calculated composition has high CaO/Na_2O and low Mg′ (0.57). Also, REE concentrations of the intercumulus melt are roughly those expected for equilibrium with plagioclase of the average cumulus composition (based on the distribution coefficients given in Table 3) (Fig. 8). We thus regard the system to be mainly an orthocumulate; i.e., the mafic component of the fragments has an average composition close to that expected for trapped cotectic melt and has incompatible-element concentrations that are too high to be mainly cumulus or adcumulus in origin. Heteradcumulus[†] pyroxene or rafted cumulus mafic grains plus adcumulus plagioclase, if present, are minor components.

Petrologic Constraints on the Precursor Igneous System

The following petrographic observations, drawn from descriptions in the Appendix, support or are permissive with respect to the proposed intercumulus crystallization of the igneous system, but add complexity to its history. Rock fragments that retain relict-igneous textures have large cumulus plagioclase grains with intercumulus pyroxene. Compositionally zoned plagioclase, the presence of ilmenite (as in 67513,7012; Appendix), and the ranges of compositions of coexisting pyroxene and plagioclase in different samples support an orthocumulus origin. In several samples, pyroxene is abundant, perhaps forming parts of localized mafic clots as is typical of anorthositic rocks (e.g., Gitlin et al., 1985). Bulk compositions of exsolved pyroxenes indicate crystallization temperatures in the vicinity of 1075–1175°C and equilibration to ≤800°C; however, the general lack of coarse exsolution textures in most samples may reflect relatively rapid subsolidus cooling.

[†] *Heteradcumulates* in this context are plagioclase cumulates containing pyroxene that crystallized from intercumulus melt, but that maintained a constant composition by adcumulus diffusion.

Table 2. Selected bulk compositions used to estimate ferroan noritic-anorthosite igneous-system composition.

	67513		67511/3	67511	67455	MAC	FNA	67513	"30/70"	Regressed values	
	All	FNA	fines	fines	bulk	88105	System	Avg	Cotectic	at 30 ppm Sc	
	(n=219)	subset				bulk	bulk	Plag	Melt	TS-INAA	INAA
notes	(1)	(2)	(3)	(4)	(5)	(6)	(7)	(8)	(9)	(10)	(11)
SiO_2				(45.0)	(44.5)	45.33	45.0	44.49	46.19		
TiO_2				0.4	0.25	0.24	0.18		0.60	0.6	
Al_2O_3	(30.0)	(29.8)	(29.6)	28.6	28.1	29.0	29.8	35.02	17.54	17.2	
Cr_2O_3	0.076	0.072	0.077	0.073	0.09	0.09	0.07		0.23	0.230	0.240
FeO	4.18	4.13	4.53	4.10	5.5	4.32	4.13	0.4	12.83	12.88	13.74
MnO				0.06	0.08	0.06	0.06		0.20		
MgO				4.0	4.05	3.89	3.00	0.2	9.53	7.91	
CaO	16.8	17.4	16.7	15.7	17.1	16.7	17.4	19.5	12.50	13.72	12.81
Na_2O	0.41	0.345	0.42	0.39	0.29	0.33	0.34	0.37	0.27		
K_2O				0.03	0.03	0.03	0.030	0.020	0.053		
P_2O_5				0.02	0.03	0.08	0.015		0.050		
Trace elements (ppm)											
Sc	8.31	8.63	8.78	8.18	11	8.47	8.63	0.3	28.1	30	30
Cr	518	495	527	500	643	638	500	10	1643	1576	1641
Co	9.3	5.8	9.2	7.2	9.3	14.5	6	0.1	20	18	21
Ni	70	9	41	55	16	150	9	2			
Sr	162	149	170	155	123	156	150	167	110	108	109
Zr	49	17	45		[17]	34	17	3	50		
Cs	0.06	0.05	0.06			0.04	0.05	0.044	0.06	0.08	
Ba	44	17.4	46	45	9.5	31	17	8	38.0	29.3	36.3
La	3.25	0.89	3.00	3.42	0.93	2.48	0.89	0.1305	2.66	2.54	2.51
Sm	1.56	0.49	1.45	1.71	0.56	1.20	0.49	0.0431	1.53	1.54	1.51
Eu	0.92	0.75	0.99	0.97	0.72	0.79	0.75	0.78	0.68		
Tb	0.33	0.11	0.31	0.39	0.14	0.25	0.114	0.006	0.37	0.38	0.37
Yb	1.24	0.50	1.2	1.34	0.6	0.99	0.496	0.016	1.62	1.64	1.64
Lu	0.17	0.071	0.17	0.19	0.095	0.14	0.071	0.002	0.23	0.24	0.24
Hf	1.17	0.36	1.09	1.24	0.39	0.9	0.36	0.008	1.18	0.92	1.06
Ta	0.14	0.04	0.14	0.19	0.07	0.11	0.043		0.14	0.10	0.12
Th	0.50	0.10	0.46	0.51	0.12	0.42	0.1		0.33	0.30	0.29
Mg' [molar MgO/(MgO/FeO)]				0.63	0.57	0.62	0.56	0.47	0.57		
CaO/Al_2O_3	0.56	0.58	0.56	0.55	0.61	0.58	0.58	0.56	0.71		

(1) Mass-weighted mean of all 219 67513 2-4 mm lithic fragments analyzed by INAA. Al_2O_3 estimated from Sc-Al correlation. (2) Mass-weighted mean of ferroan noritic-anorthosite (FNA) subset of sample 67513 lithic fragments, defined as those that have Sm < 2 ppm minus those that have Sc/Sm < 5 and Sm > 1 ppm (148 particles or 70 wt.% of total analyzed). (3) Mass-weighted mean of 143 mg of 67511 <1 mm fines and 408 mg of 67513 "abrasion" fines. (4) Composition of bulk 67511, KOROTEV (1982), SiO_2 estimated. (5) Bulk composition of feldspathic fragmental breccia 67455, LINDSTROM and SALPAS (1981). SiO_2 and other bracketed values from WÄNKE et al. (1975) (6) Antarctic meteorite from lunar highlands, MAC88105, shown for comparison. Bulk chemical composition from JOLLIFF et al. (1991a). (7) Composition of FNA igneous system derived from values of column 2 and major elements not analyzed by INAA derived from samples for which major elements were analyzed by electron-microprobe analysis of fused beads. (8) Average cumulus plagioclase trace-element composition derived from 67513,7071; 7075; 7052; 7159. See text for major-element derivation. Composition corresponds to An value of 96.6. (9) Cotectic (intercumulus) melt coexisting with cumulus plagioclase; calculated by subtracting 70% cumulus plagioclase from bulk "FNA system" composition. Columns 10 and 11 are meant for comparison to the values given in column 9. (10) Concentrations calculated by linear regression against Sc concentration at 30 ppm for lithic fragments from sample 67513 whose ferroan-suite character, as defined by Mg' of pyroxene and olivine, and An content of plagioclase, has been confirmed in thin section (TS) by electron-microprobe analysis. (11) Concentration values calculated by linear regression against Sc concentration at 30 ppm Sc for all 148 lithic fragments in 67513 analyzed by INAA that we have included in the ITE-poor, FNA suite.

Plagioclases clouded with mafic inclusions may be incipiently exsolved, owing to very slow cooling, but not completely cleared by any late recrystallization, as appears to have happened for many of the sampled lunar ferroan anorthosites (Smith and Steele, 1974; Dixon and Papike, 1975). The inclusion-rich nature of plagioclase in these samples suggests that, at high temperatures, the dissolved Fe and Mg concentrations in the plagioclases were significantly higher than at present. Irregular, patchy zoning, irregular crystal shapes, and inclusion-rich regions in plagioclase indicate partial resorption and reequilibration, at least of mafic components, within plagioclase. Spinel "necklaces" within large pyroxene grains and outlining parts of relict pyroxene crystal surfaces reflect variable resorption and growth of host pyroxenes as might result from crystallization in more than one episode under different conditions.

Together, these characteristics reflect a complex cooling history, consistent with a large magmatic system in which plagioclase initially accumulated within a perched layer (e.g., Morse, 1982). Two episodes of pyroxene crystallization might result from early pyroxenes having begun crystallization in a relatively deep system, but which subsequently became unstable and were partially resorbed. Later, pyroxenes continued growth as an intercumulus phase when porosity or communication with the magma reservoir were restricted, leading to orthocumulus textures. Subcalcic augite and pigeonite of calcic bulk composition, containing abundant, crystallographically oriented oxide inclusions, suggest deep ori-

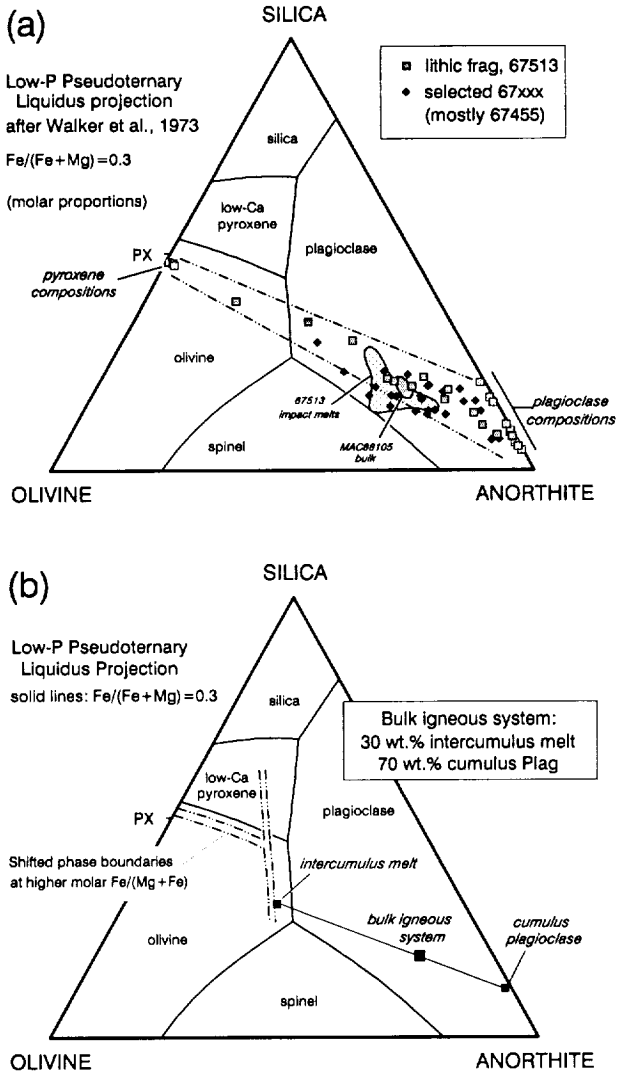

FIG. 4. Low pressure pseudoternary liquidus projection onto the plane olivine-silica-anorthite in molar proportions, after Walker et al. (1973). (a) Major element compositions of rock fragments from 67513 and other selected ferroan compositions from Station 11, mostly subsamples from 67455 (Ryder and Norman, 1979; Lindstrom and Salpas, 1981). Selected plagioclase and pyroxene compositions determined with the electron microprobe are plotted (lighter-stippled squares) to show where actual mineral compositions plot on this diagram. The high silica concentration of albite relative to anorthite displaces plagioclase compositions slightly toward the silica apex. MAC88105 lunar-highland meteorite composition shown for comparison (from Jolliff et al., 1991a). (b) Bulk composition of ferroan noritic-anorthosite (FNA) composition igneous system derived from sample 67513 lithic fragment compositions. Intercumulus-melt composition derived from mass balance given our interpretation of the system as a mixture of 70% cumulus plagioclase and 30% intercumulus melt (cf. Morse, 1982, his Fig. 5). Solid phase boundaries are for Fe/(Fe + Mg) = 0.3. Dashed phase boundaries illustrate shift caused by increased Fe/(Fe + Mg) after the method of Longhi (1991).

gins (i.e., that oxide components were once dissolved in the pyroxene). However, the lack of coarse pyroxene exsolution textures may be consistent with a two-stage history involving late-stage cooling in a shallower plutonic environment.

The modes of igneous assemblages in both monomict and polymict fragments correspond to the following rock types: anorthosite, noritic anorthosite, anorthositic norite, norite, and gabbronorite (classification of Stöffler et al., 1980). These are the rock types we would expect to find among fragments from the anorthositic layers of mafic layered intrusions such as the Middle Banded Zone of the Stillwater Complex (McCallum et al., 1980; Salpas et al., 1983; Gitlin et al., 1985; Haskin and Salpas, 1992) or from layers of anorthosite and leucogabbro in a rock body such as the Archean Fiskenaesset Complex in Greenland (Weaver et al., 1981) or the Bad Vermilion Lake Complex, Ontario (Morrison et al., 1987).

In addition to bulk geochemical characteristics, mineral compositions and the inferred order of crystallization also suggest a magmatic relationship among the different mineral assemblages. All of the assemblages are ferroan, and the An contents of the plagioclases generally correlate with Mg′ values of accompanying mafic silicates to form a trend consistent with progressive crystallization from a single starting composition (Jolliff, 1992a). Augite, although not abundant, is present in many samples, and pigeonite is relatively calcic. These features require some process such as crystallization of a magma sufficiently calcic that early assemblages of plagioclase and olivine ± orthopyroxene allow the $CaSiO_3$ component of residual liquids to increase, eventually bringing calcic pigeonite, or augite plus pigeonite, onto the liquidus. Spinel is a common accessory mineral and is typically Cr-rich. Ilmenite is rare, but where present, is of similar composition (i.e., uniformly low Mg′).

Other workers have suggested that certain sets of rocks collected at the rim of North Ray Crater derived from a single, igneous precursor. Lindstrom and Salpas (1981) speculated that clasts from feldspathic fragmental breccia 67455 derived from impact into rocks of a single igneous suite of ferroan anorthosite and gabbroic anorthosite or some other unspecified mafic rock, and that the associated melt rocks represent the bulk composition of that suite. Petrologists who have examined anorthositic breccia 67075 have concluded that it formed by fragmentation and mixing of related plutonic igneous rocks such as those of the leucocratic parts of a layered igneous complex, i.e., was genomict (e.g., Peckett and Brown, 1973; McCallum et al., 1975).

Solidification of the Ferroan Noritic-Anorthosite Igneous System

Our model for the formation of these rocks begins with cumulus plagioclase, which could have formed as envisioned by Morse (1982). In that model, plagioclase nucleates within a magma and accumulates upward as a buoyant layer (Fig. 9). Mafic minerals crystallizing with plagioclase in the zone of nucleation sink and become separated from plagioclase. The accumulating layer of plagioclase is porous and the pores are filled with intercumulus melt. We accept the initial presence of cumulus plagioclase and intercumulus melt; we do not consider in detail their origin. We do not presume that the intercumulus melt and cumulus plagioclase were initially at equilibrium with each other, merely that they were in contact when the system effectively became closed to further exchange of melt.

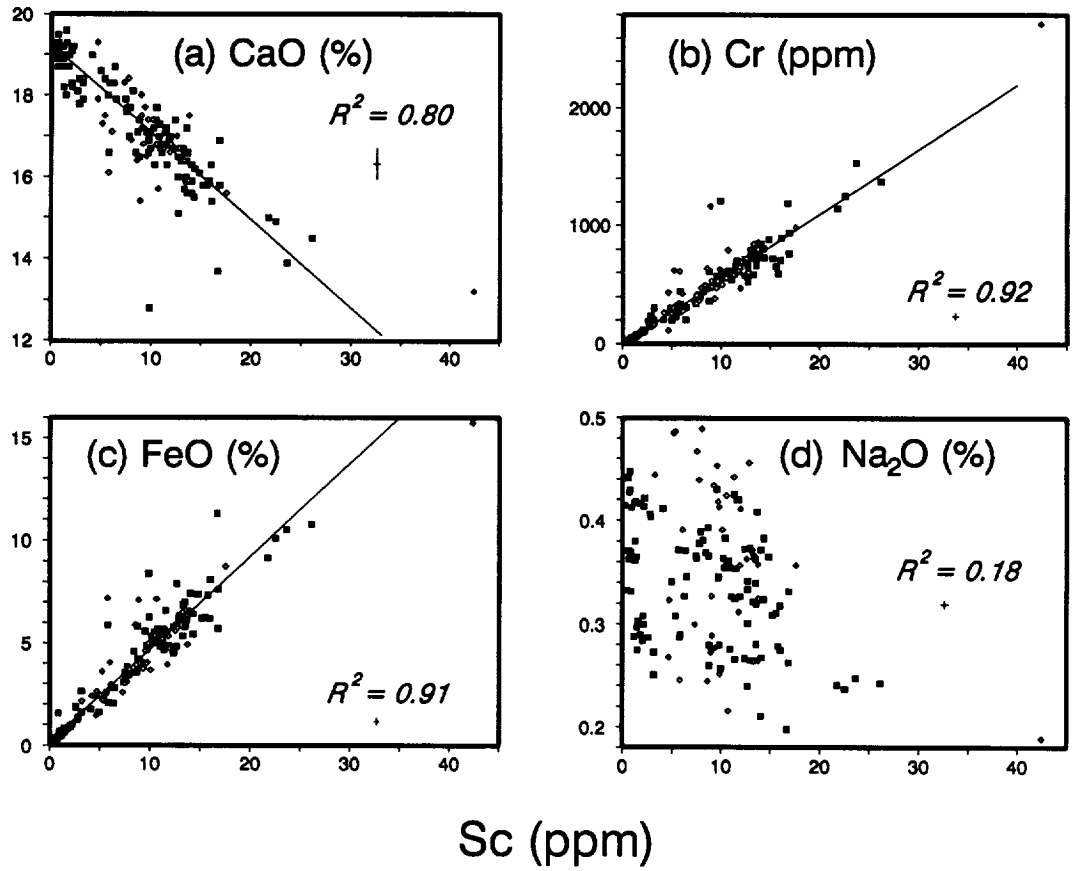

FIG. 5. Concentrations of Sc vs. (a) CaO, (b) Cr, (c) FeO, and (d) Na_2O in ITE-poor group of lithic fragments from sample 67513. Data are from INAA; the total number of data points is 148. Regression lines are determined in order to estimate "endmember" mixing components for those elements whose concentrations are well correlated with those of Sc (see text). Regression lines are based only on data points represented by square symbols; these are the samples that fall most closely along the Sc-Sm correlation line. Total number of regressed data points is 112. The range of concentrations of Na_2O at low Sc concentrations indicates the presence of more than one plagioclase component among these samples. The analytical uncertainty is shown by the "cross" symbol for the average concentrations, at about 10 ppm Sc.

We consider initially two simple, but extreme, crystallization models for intercumulus melt to determine the compositions of successive solids and evolved residual liquids. Both assume the cumulus plagioclase is refractory and unreactive. The first model is simple equilibrium crystallization of intercumulus melt within the plagioclase framework. On solidification, the intercumulus melt produces a solid of its own composition. The second model is based on fractional crystallization, which we approximate as a series of equilibrium crystallization steps, each beginning with the residual liquid from the previous step. As crystallization takes place, the two components being produced from intercumulus melt, postcumulus solid and more evolved residual liquid, may become partially separated from each other by migration of melt or by armoring of early-forming solids. As the separation can take place at any stage during crystallization, a range of solid and residual liquid compositions is produced. In this model, successive liquids are in equilibrium only with the solid from the previous increment of crystallization, not with all solid previously produced from the starting liquid. Presumably, in the natural system, there was continuous, but imperfect, small-scale equilibration between successively crystallizing assemblages, which yielded crystallization products intermediate to those we model by simple equilibrium and stepwise (fractional) crystallization.

We have used the crystallization programs MAGFOX and MAGPOX developed by Longhi (1977, 1978, 1980, 1987, 1991) to track quantitatively the composition of derivative residual liquids and solids in systems consisting of plagioclase, olivine, pyroxenes, and residual melts at relatively low pressures ($\leq$2 kbar). We have combined the calculations of compositions of residual melts and solids with calculations of corresponding trace-element compositional evolution and system mass balance in order to model the crystallization of intercumulus melt.

Equilibrium Crystallization

We model the concentrations of representative trace elements (Sc, Ba, La, Sm, Eu, Tb, and Yb) of residual liquids

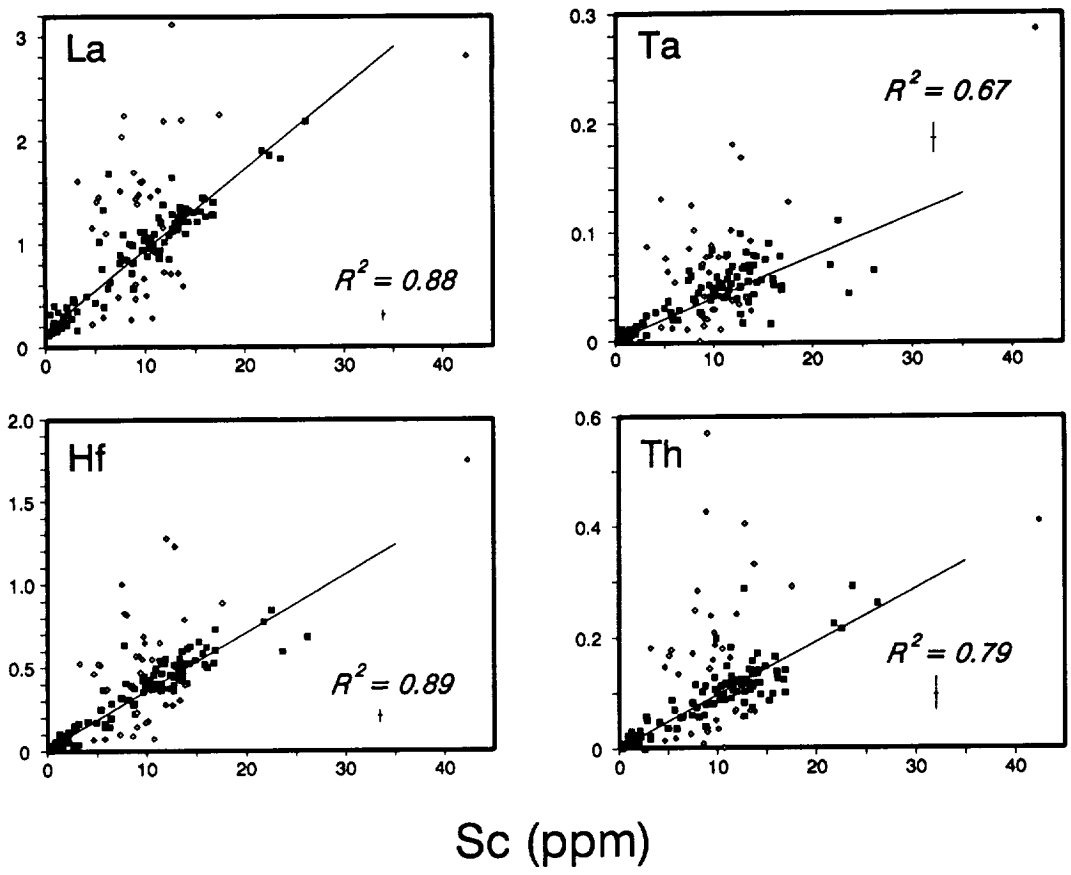

FIG. 6. Concentrations of incompatible trace elements vs. Sc concentrations in the ITE-poor group of lithic fragments from sample 67513. Data are from INAA; the total number of data points is 148. Regression lines are based only on data points represented by square symbols; these are the samples that fall most closely along the Sc-Sm correlation line. Total number of regressed data points is 112. The analytical uncertainty is shown by the cross symbol for the average concentrations, at about 10 ppm Sc.

and solids based on equilibrium with the solid assemblages calculated by the program MAGPOX at specified intervals during crystallization. We use the following equation, in the notation of Beattie et al. (1993), for batch equilibrium crystallization (e.g., Eqn. 4.7, Haskin, 1984, for derivation): $C_i^L = C_i^{L,0}/(\bar{D}_i(1 - F) + F)$ where $C_i^{L,0}$ is the initial concentration of element i in the original melt, C_i^L is its concentration in the residual liquid, F is the fraction of melt remaining, and $\bar{D}_i$ is the bulk distribution coefficient for element i calculated as $\bar{D}_i = \sum_{j=1}^{n} \phi^j D_i^j$ for all minerals j, where ϕ^j is the weight fraction of mineral j in the equilibrium solid. Values of distribution coefficients (D_i^j) used in our modeling are given in Table 3. Distribution coefficients for the REEs in the pyroxenes are correlated with their Wo contents (McKay et al., 1986); we calculate them from the equation $\log(D) = A \times \text{Wo} - B$, using constant values for A and B from McKay et al. (1986).

The evolution of the mineral assemblage of postcumulus solids produced by equilibrium crystallization of intercumulus melt is shown in Fig. 10a. Initial intercumulus crystallization of plagioclase and olivine is followed by crystallization of low-Ca pyroxene and partial resorption of olivine. Pigeonite is the stable pyroxene, crystallizing after some 30 wt% solidification of intercumulus melt; augite crystallizes only after about 70% solidification (Fig. 10a). Compositions of equilibrium liquids and solids at intervals of 25, 50, 75, 90, and 95% crystallization are given in Table 4. The Sc concentrations of postcumulus solids (i.e., not including cumulus plagioclase) increase to about 28 ppm at very low Sm concentrations (Fig. 11a); Sc becomes compatible in the solid assemblage only when pyroxene begins to crystallize. Concentrations of Sc and Sm in instantaneous solid compositions follow a trend that initially and during most of the postcumulus crystallization interval lies below the main trend of rock fragments in 67513 (Fig. 11b). Concentrations of REEs in residual liquids increase from initial values of ~8 times chondrites for La and 7 times for Yb to >100 times for La and ~75 times for Yb at 95% crystallization (Fig. 12a). The products of intercumulus-melt crystallization are relatively mafic assemblages ranging from troctolitic (25% crystallization) to gabbroic (90% crystallization).

To a first approximation, simple equilibrium crystallization yields a postcumulus solid assemblage at full crystallization

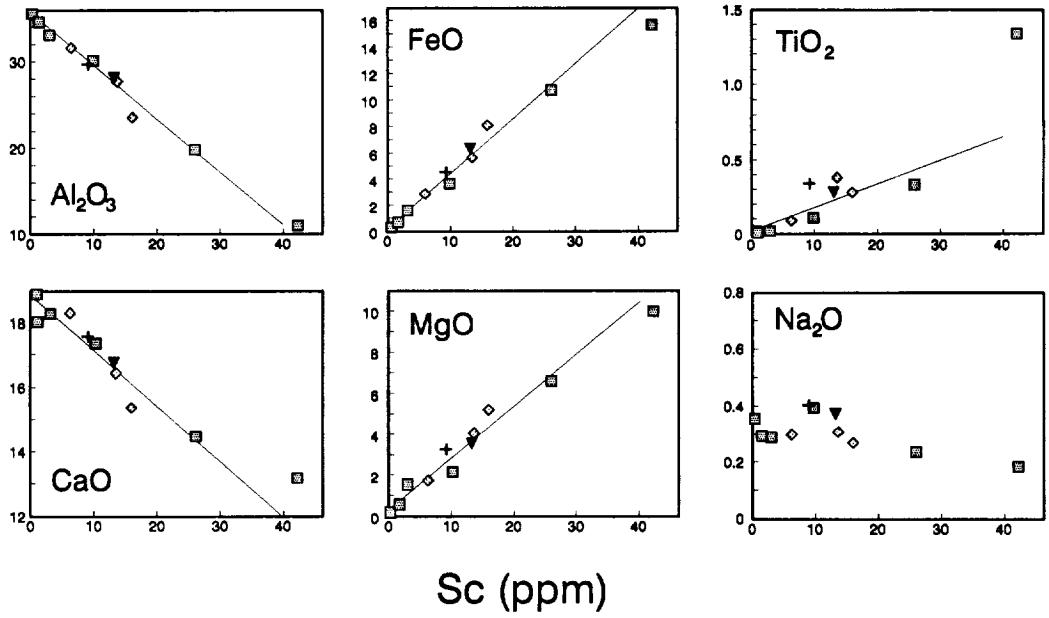

FIG. 7. Concentrations of oxides vs. Sc in ITE-poor samples from 67513 that were analyzed for major elements by electron-microprobe analysis of fused beads (Table 1). Symbols: squares, igneous fragments; triangles and diamonds, fragmental breccias; cross, impact-melt breccia. Lines fit by linear regression, excluding 67513,7012 (outlier at 42.4 ppm Sc). The purpose of the regression lines is to estimate the concentrations of each element at about 30 ppm Sc to test how well the regressed value matches our independently estimated intercumulus-melt composition. Regressed values for these oxides and for trace elements are given in Table 2. The good correlations for most elements are taken as evidence that these samples derived from mixtures of plagioclase (Sc-poor end) and intercumulus melt (Sc-rich end).

that, when mixed with cumulus plagioclase, accounts for much of the distribution of intermediate bulk compositions of the lithic fragments. The paucity of olivine overall and the absence of olivine-rich samples suggest that equilibrium crystallization prevailed during the early phase of intercumulus-melt crystallization. The major shortcoming of the simple equilibrium crystallization model is that the compositions of coexisting pyroxene and plagioclase of modeled postcumulus solids do not match those of the samples; Mg′ values of pyroxene do not extend low enough (e.g., the calculated equilibrium value for orthopyroxene of ~0.59 vs. observed range of ~0.48–0.65), and plagioclase An contents are lower than observed (calculated equilibrium value of ~94.5 vs. observed range of ~94.5–96.8; see Fig. 13). Nevertheless, the major mineral sequence predicted by this model is similar to the one observed. Pyroxene and plagioclase dominate the crystallization products, as expected for equilibrium crystallization of cotectic melt whose bulk composition lies close to the pyroxene-plagioclase join.

Fractional Crystallization

To obtain a greater range of postcumulus solid and liquid compositions, we model the crystallization of intercumulus melt in four crystallization intervals and three melt-separation steps, at 25, 50, and 75% solidification, taking the residual liquid from each step as the starting liquid composition for the subsequent step. Then we examine the compositions obtained by equilibrium crystallization of the liquid following the third (75%) step at 90 and 95% total solidification (with no further separation of solids). Changes in the mode of postcumulus solids are shown in Fig. 10b (see Table 5). Plagioclase and olivine crystallize initially, followed by spinel, then pigeonite joins the assemblage, and augite crystallizes at ~75% solidification. Ilmenite appears late, after ~90% crystallization of intercumulus melt (i.e., <3% of the total system remaining as melt), consistent with the observation that it is present only in the most compositionally evolved assemblages (lowest Mg′ and An values).

The evolution of trace-element concentrations in residual liquids is similar to that for single-step equilibrium crystallization but covers a wider range of compositions (Fig. 11a). One consequence of the isolation of early-formed postcumulus plagioclase and olivine is that later-formed postcumulus solids reach higher Sc concentrations than those produced by simple equilibrium crystallization (about 45 ppm for pyroxene-bearing assemblages; Fig. 11b). This is especially true for assemblages formed at >50% crystallization. In the event of migration of part of the liquid, or incomplete sampling of the local mineral assemblage, a particular analyzed rock fragment may consist of cumulus plagioclase, postcumulus mineral assemblages crystallized from intercumulus melt (locally troctolitic to gabbroic), small amounts of frozen, evolved trapped liquid, or combinations of these.

On the size scale of our samples, we might expect to see substantial deviation of compositions of individual fragments away from the simple mixing line between cumulus plagioclase and intercumulus melt. The compositions of most, however, lie close to the well-correlated group (e.g., Fig. 11b), indicating that there was either little physical separation of

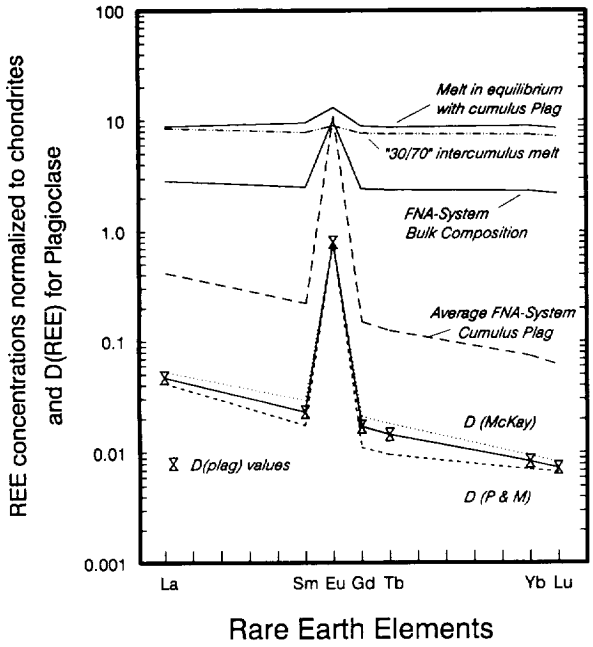

FIG. 8. Chondrite-normalized REE concentrations of model components of the ferroan noritic-anorthosite system. The calculated composition of melt in equilibrium with average cumulus plagioclase and the intercumulus-melt composition calculated assuming 30% intercumulus melt and 70% cumulus plagioclase are shown (see also Table 2). Values of REE distribution coefficients used for plagioclase are also plotted (from McKay, 1982; Phinney and Morrison: "P & M," 1990).

solids from residual liquids on the size scale of the fragments or that most of them regained a nearly average fraction of trace elements during breccia formation, despite their small size. It is presumably the fragments whose compositions lie off the line that gained or lost residual liquids by migration after postcumulus solidification had begun.

As was the case with the equilibrium model, mineral compositions predicted by the stepwise crystallization model do not acceptably match those of the samples that we interpret to be part of the orthocumulus trend (Fig. 13). In the late stages of crystallization, the model predicts postcumulus solids and residual liquids that have very low values of Mg′ (Table 5), as required to match some of the samples, but modeled early-formed assemblages contain mafic silicates that are more magnesian than any observed in the samples (calculated orthopyroxene Mg′ as high as 0.80 vs. observed ~0.65 maximum). We suspect that early-formed olivine and pyroxene equilibrated easily with evolving residual liquids, closely approaching the case of equilibrium crystallization. For the mafic minerals, we conclude that the two crystallization models, equilibrium crystallization and stepwise fractional crystallization, approximately bracket the conditions that prevailed in different regions of the system. Plagioclase, however, remains a problem. Modeled compositions of plagioclase crystallizing from intercumulus melt are more sodic than those we observe; orthocumulus plagioclase is about one An unit too low (Na_2O ~ 20% too high). We consider two possible reasons for this discrepancy: (1) the Na_2O concentration of our cumulus plagioclase model component is too low, or (2) partial equilibration occurred between intercumulus melt or intercumulus plagioclase and cumulus plagioclase.

If the Na_2O concentration chosen for the cumulus plagioclase component is too low, our model yields (by mass balance) a Na_2O concentration of the intercumulus melt that is too high. For the crystallization models described above, the intercumulus melt Na_2O concentration was based on a cumulus plagioclase Na_2O concentration of 0.37 wt%, but this produced equilibrium intercumulus plagioclase about one An unit lower than observed in the "orthocumulus trend." If we take the average Na_2O concentration of cumulus plagioclase to be higher (see examples in Fig. 13 at 0.39 and 0.41 wt%), then the final (endstage) intercumulus plagioclase has Na_2O in the observed range, but the initial, equilibrium intercumulus plagioclase is more calcic than the average cumulus plagioclase. Another way to explain low Na_2O concentrations in intercumulus material is by partial equilibration of crystallizing intercumulus melt or intercumulus plagioclase with part of the adjacent cumulus plagioclase.

Cumulus Plagioclase Recrystallization and Reequilibration

The crystallization of intercumulus melt occurs in the presence of cumulus plagioclase, which in effect provides the

Table 3. Distribution coefficients used in crystallization modeling.

	Olivine	Plagioclase	Orthopyroxene	Pigeonite	Augite	Ilmenite
Sc	0.265 (1)	0.012 (cf 2,11)	1.4 (1)	2.5 (3)	3.9 (2)	2.2 (4)
Ba	0.001 (5)	0.15 (5-7)	0.011 (1)	0.016 (3)	0.02 (8)	0.005 (16)
La	0.0001 (9)	0.047 (10,11)	0.0004 (15)	0.001 (13)	0.05 (13)	0.005 (5)
Sm	0.001 (9)	0.023 (10,11)	0.007 (15)	0.013 (13)	0.23 (13)	0.01 (5)
Eu	0.0009 (9)	0.8 (12)	0.01 (14)	0.01 (14)	0.22 (13)	0.007 (5)
Tb	0.0024 (9)	0.0144 (10,11)	0.011 (15)	0.019 (13)	0.26 (13)	0.02 (5)
Yb	0.02 (9)	0.0083 (10,11)	0.063 (15)	0.085 (13)	0.31 (13)	0.075 (5)

(1) MCKAY and WEILL (1977); (2) LINDSTROM (1976); (3) Estimated from augite and orthopyroxene; (4) IRVING et al. (1978); (5) MCKAY and WEILL (1976); (6) BLUNDY and WOOD (1991); (7) DRAKE and WEILL (1975); (8) GILL (1979); (9) MCKAY (1986); (10) MCKAY (1982); (11) PHINNEY and MORRISON (1990); (12) WEILL and MCKAY (1975); (13) Calculated as discussed in text, based on MCKAY et al. (1986). Values shown are examples calculated for Wo=0.06 (pigeonite) and Wo=0.40 (augite). (14) MCKAY et al. (1990); (15) REE in orthopyroxene calculated as for pigeonite, at low wollastonite content (example at Wo=0.2). (16) Assumed, cf. LONGHI (1980); SNYDER et al. (1992).

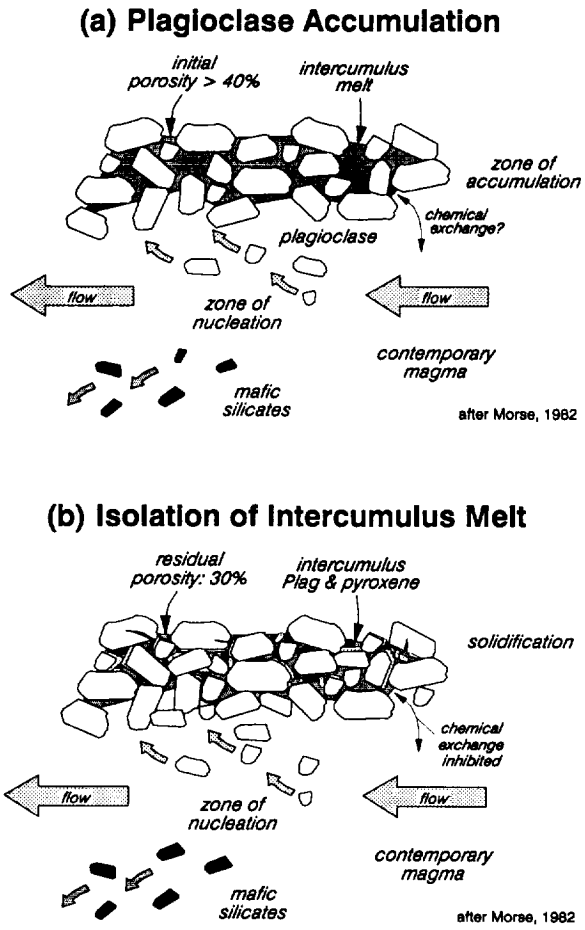

FIG. 9. Schematic illustration of formation of cumulus plagioclase and intercumulus melt system as we envision for the precursor of lithic fragments in sample 67513. Models are based on those of Morse (1982). Plagioclase accumulates as a suspension-cumulate layer within a large magma reservoir, separated from cogenetic mafic cumulates by density contrasts. In this particular case, we postulate that when the residual porosity reached 30%, chemical exchange with the contemporary magma reservoir was inhibited.

walls of the crystallization chamber for each local parcel of intercumulus melt. That the An content of postcumulus plagioclase of lunar ferroan anorthosites was "buffered" by the An content of cumulus plagioclase was proposed by Raedeke and McCallum (1980) to explain the highly and uniformly calcic plagioclase compositions despite variable Mg′ of coexisting mafic silicates (see also Longhi and Boudreau, 1979; James, 1988). Morse (1984), however, has argued against simple reequilibration of Na_2O by solid-state diffusion in cumulus plagioclase because of the extremely sluggish tetrahedral Al ⇔ Si exchange in plagioclase that would accompany Na ⇔ Ca exchange. Nevertheless, many characteristics of lunar plagioclase seem to require some postcumulus change in anorthositic rocks and their plagioclase. Evidence for this includes the very low Fe and Mg concentrations in plagioclase, similar to terrestrial plagioclase that has undergone granulite metamorphism (Phinney, 1991, 1994); plagioclase that has exsolved mafic components (Nord, 1976; Smith and Steele, 1974), and recrystallization textures (Stewart, 1975; James, 1980). Despite the fact that solid-state exchange is so slow, we think that some exchange of Na, Ca, and other elements between original, cumulus plagioclase and crystallizing intercumulus melt, or its products must have occurred.

Although we do not know the mechanism of exchange or reequilibration, we observe plagioclase grains that have exsolved mafic components and whose compositions are consistent with a process of at least partial reequilibration. Plagioclases in ferroan anorthosites in general and in many of the lithic fragments of sample 67513 have very low MgO concentrations and Mg′ values ranging from 0.5 to near zero

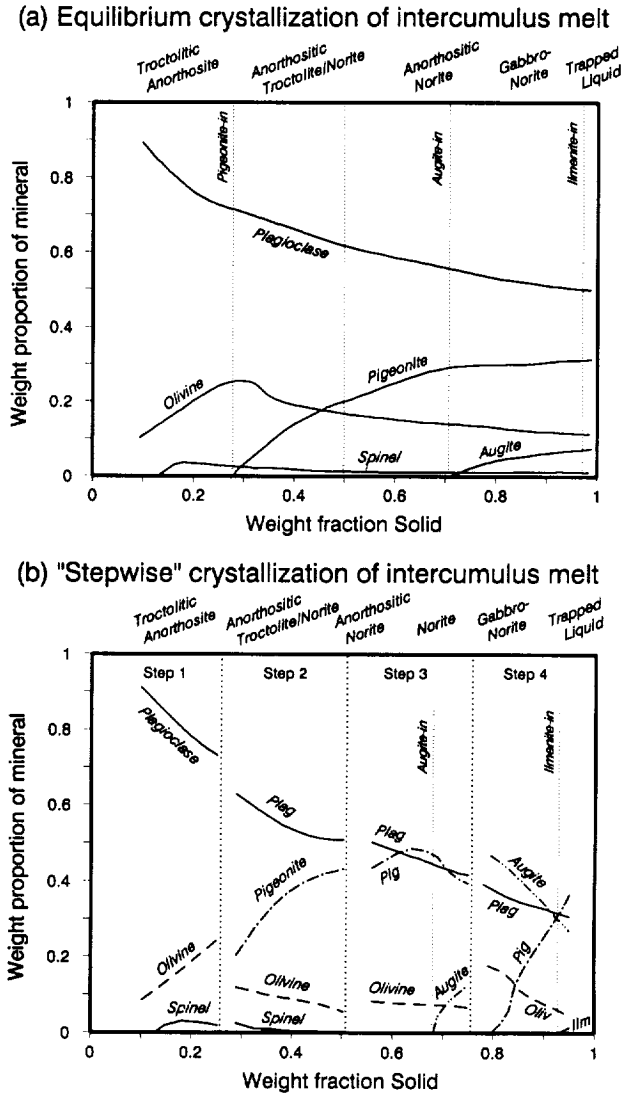

FIG. 10. Weight proportions of minerals crystallized as a function of the weight-fraction solid during crystallization of the ferroan noritic-anorthosite system. (a) Model results of equilibrium crystallization of intercumulus melt assuming the system consists of 70% cumulus plagioclase and 30% intercumulus melt. (b) Model results of stepwise crystallization (four steps) of the "30%" intercumulus melt. Discontinuities are caused by abrupt separation of melt and solid at 25, 50, and 75% crystallization steps.

(Papike et al., 1991). Given D values (plag/melt) of 0.033 and 0.040 for Fe^{2+} and Mg, respectively (Longhi et al., 1976; Phinney and Morrison, 1990; Phinney, 1992), plagioclase in equilibrium with cotectic melt should have FeO and MgO concentrations on the order of several tenths of a weight percent each, easily measurable by electron-microprobe analysis. That most of the plagioclases have low to very low MgO concentrations (e.g., <0.1 wt%) suggests that they have partially reequilibrated with evolved residual liquid of ferroan composition or that they have experienced subsolidus recrystallization or exsolution of mafic silicates at some temperature below their original crystallization temperature for which the D value for Mg (and possibly Fe^{2+}) is reduced significantly. One of these processes may cause the observed "trend" at high An content (An 96.5–98.0) in Fig. 13, but we defer discussion of this for the present.

As additional evidence for partial reequilibration of cumulus plagioclase, we find grains of irregularly zoned, relatively coarse plagioclase whose zonation spans a factor of two or more in Na_2O concentrations. In most samples, however, plagioclases are cataclastic, or they occur as fragments juxtaposed within breccia, so the textural evidence is ambiguous as to whether most of them are relicts of partial recrystallization and reequilibration. We also find grains of plagioclase that are in contact with pyroxene and that are compositionally zoned, with the bulk of the grains having $\sim An_{96.5}$ composition, but with "islets" of composition as much as one An unit higher, within large plagioclase grains. While these may be relicts of igneous zoning, the zoning is not regular. These grains have low bulk FeO and MgO concentrations, less than those of the cumulus plagioclase model component, which, from the standpoint of equilibrium with cotectic melt, represent a more plausible initial igneous composition.

Phinney (1991) has argued on the basis of compositional and textural evidence that most, if not all, plagioclases of lunar ferroan anorthosites have recrystallized to some extent, thus facilitating equilibration. Recrystallization of some sort has facilitated loss of Fe and Mg at some subsolidus temperature in plagioclases of both lunar and terrestrial granulitic rocks (Phinney, 1991, 1994). In the samples of this study, we observe granular exsolution of mafic minerals from plagioclase frozen in the process of recrystallization. We also observe plagioclase without inclusions but with extremely low FeO and MgO concentrations. Some samples have granoblastic domains within coarse plagioclase grains, a clear indication of recrystallization. This may have been triggered by strain introduced from movement of the anorthositic system as a diapir, perhaps while the intercumulus material was partially molten, to a higher crustal level, or by shock from meteorite

Table 4. Equilibrium crystallization model compositions.

	"30/70"	25% Cryst'd		50% Cryst'd		75% Cryst'd		90% Cryst'd		95% Cryst'd	
	Cot Mlt	Melt	Solid	Melt	Solid	Melt	Solid	Melt	Solid	Melt	Solid
percent:	100	75	25	50	50	25	75	10	90	5	95
					Oxides (wt.%)						
SiO_2	46.19	47.59	42.50	47.13	45.20	46.37	46.13	45.16	46.30	43.35	46.33
TiO_2	0.60	0.82	0.03	1.12	0.05	2.12	0.09	4.31	0.20	6.51	0.32
Al_2O_3	17.54	14.36	25.92	13.11	22.20	11.43	19.59	10.77	18.27	10.00	17.90
Cr_2O_3	0.23	0.14	0.48	0.14	0.33	0.14	0.26	0.14	0.24	0.14	0.24
FeO	12.83	15.48	5.84	17.58	7.83	19.31	10.66	19.98	12.06	20.40	12.47
MnO	0.20	0.25	0.08	0.28	0.11	0.32	0.16	0.33	0.19	0.34	0.19
MgO	9.53	9.15	10.54	7.81	11.35	5.82	10.78	4.86	10.04	4.66	9.77
CaO	12.50	11.80	14.35	12.34	12.66	13.84	12.05	13.35	12.41	12.83	12.48
Na_2O	0.270	0.275	0.257	0.286	0.253	0.290	0.263	0.295	0.267	0.278	0.269
K_2O	0.053	0.070	0.008	0.093	0.011	0.162	0.016	0.290	0.027	0.390	0.037
P_2O_5	0.050	0.07	0.00	0.10	0.00	0.20	0.00	0.51	0.00	1.10	0.00
					Trace elements (ppm)						
Sc	28	37	2.9	36	20	32	27	28	28	27	28
Cr	1643	950	3290	957	2264	976	1801	973	1660	947	1624
Ba	38	50	5.6	68	6.7	120	10.6	220	18	294	26
La	2.66	3.62	0.131	5.04	0.154	9.82	0.262	21.9	0.591	37.3	1.03
Sm	1.53	2.10	0.038	2.94	0.051	5.77	0.112	12.3	0.377	19.9	0.67
Eu	0.68	0.77	0.448	0.90	0.451	1.16	0.519	1.41	0.602	1.52	0.64
Tb	0.37	0.50	0.007	0.70	0.009	1.39	0.024	2.93	0.090	4.70	0.16
Yb	1.62	2.22	0.029	3.08	0.073	5.78	0.221	10.9	0.619	15.5	0.96
Mg'	0.57	0.51	0.76	0.44	0.72	0.35	0.64	0.30	0.60	0.29	0.58
					Weight fractions of minerals in solid assemblages						
Olivine			0.251		0.167		0.133		0.121		0.116
Plagioclase			0.729		0.626		0.555		0.516		0.508
Pigeonite					0.197		0.300		0.306		0.312
Augite							0.008		0.053		0.060
Spinel			0.020		0.010		0.005		0.004		0.004
					Mineral component fractions						
Plagioclase An			0.968		0.963		0.956		0.951		0.948
Olivine Fo			0.77		0.72		0.63		0.58		0.57
Pigeonite Mg'					0.74		0.65		0.60		0.59
Augite Mg'							0.71		0.66		0.64

Cotectic (intercumulus) melt composition from Table 2. Crystallization is at 2kb pressure (~40 km on the Moon). Derivative melt and solid proportions are given in weight percent.

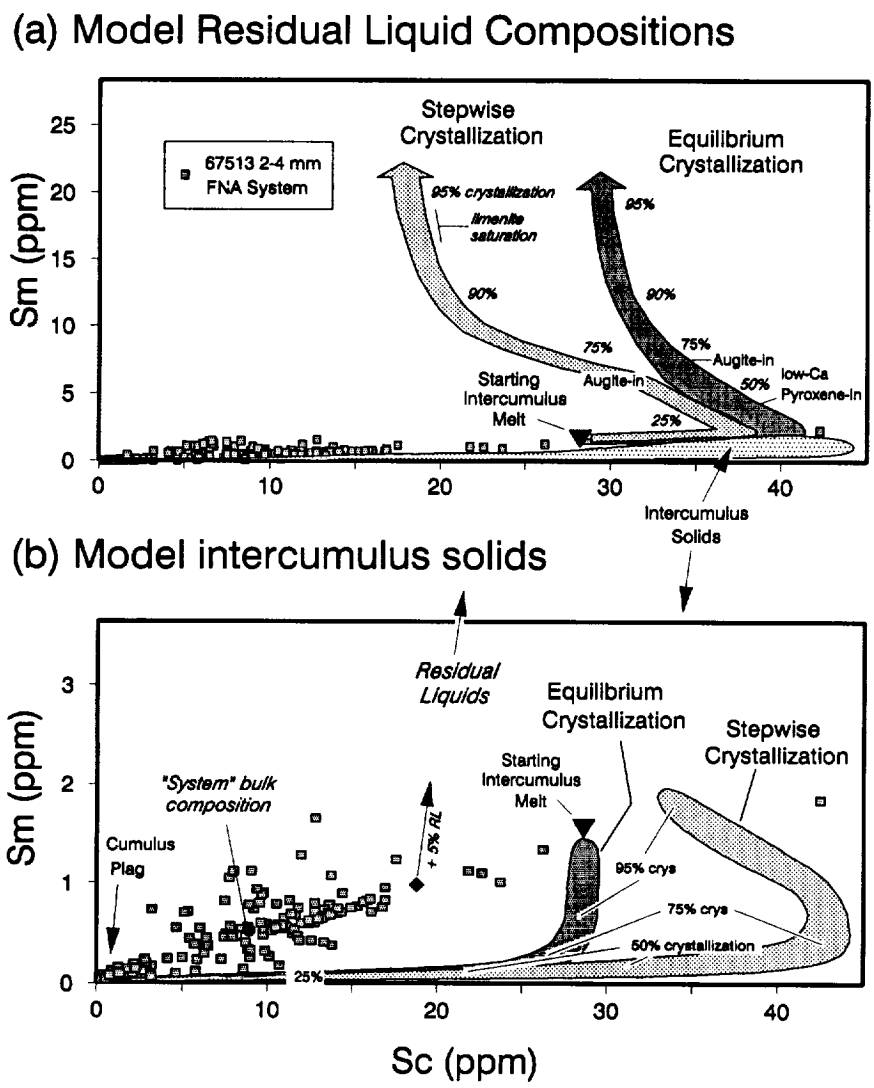

FIG. 11. Scandium vs. Sm concentrations of modeled residual liquids and intercumulus assemblages (stippled fields) compared to compositions of FNA-system lithic fragments from sample 67513 (squares). (a) Compositional evolution of residual liquids during crystallization of intercumulus melt. (b) Compositional evolution of intercumulus solids (note expanded Sm axis). The equilibrium crystallization model does not produce Sc concentrations of intercumulus assemblages that exceed that of the starting intercumulus melt composition, whereas the step-wise crystallization model yields more Sc-rich pyroxene-bearing assemblages. Mixing of different proportions of cumulus plagioclase, intercumulus solids, and residual liquids would lead to a variety of possible rock compositions that scatter about the main trend. For example, the effect of adding 5% of residual liquid (RL), taken as that at 95% equilibrium crystallization of intercumulus melt, is shown by the short vector for a hypothetical sample composition at about 18 ppm Sc.

impact followed by prolonged residence in a high-temperature environment.

Distribution of Mafic Minerals in Precursor Igneous Rocks

In this section, we consider whether the observed mafic assemblages, as recorded by the pyroxene-rich lithic fragments, might have been part of a single noritic-anorthosite lithology, or whether they might have been noritic or gabbroic layers within an anorthositic body. Perhaps mafic mineral assemblages formed "clots" within the plagioclase matrix, as observed in some terrestrial anorthosites, typically on a scale much larger than the size of our samples (e.g., Stillwater anorthosites; Gitlin et al., 1985; Haskin and Lindstrom, 1988). Whether or not the mafic assemblages were intimately mixed with cumulus plagioclase is important with respect to reaction between intercumulus components and cumulus plagioclase, as suggested above.

The distribution of Sc concentrations in the samples (Fig. 14), which essentially represents the distribution of the mafic assemblages, is consistent with an intimate mixture of cu-

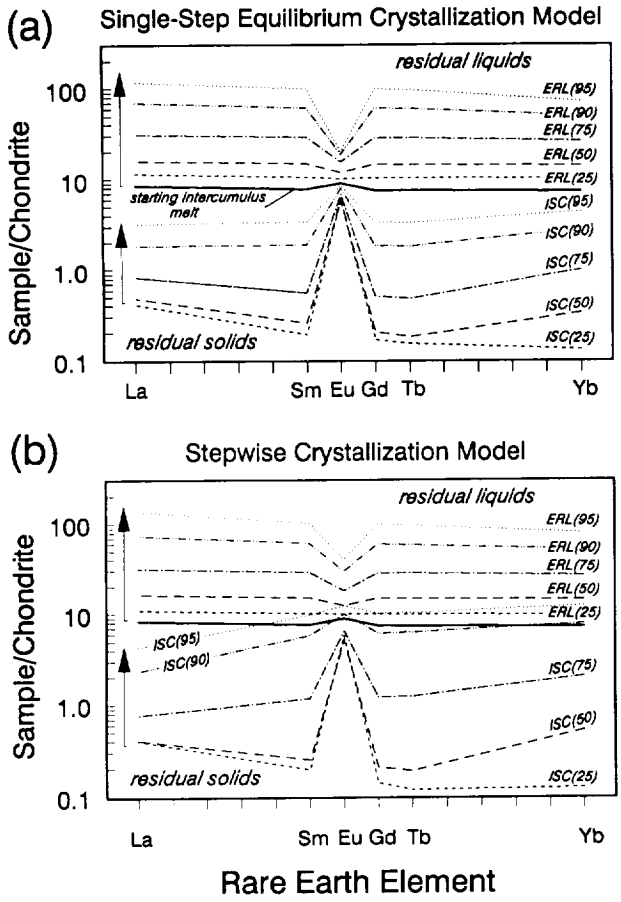

FIG. 12. Chondrite-normalized REE concentrations of model instantaneous solid compositions (ISC) and equilibrium residual liquids (ERL) at selected intervals during (a) single-step equilibrium crystallization; (b) stepwise crystallization.

mulus plagioclase and intercumulus material. Fragments rich in cumulus plagioclase are present, as indicated by the peak on the histogram at low Sc concentrations. This requires some plagioclase-rich regions in the igneous protolith and that fragments of it survived the brecciation process intact. The other peak of the histogram is broader and contains the majority of the samples; it lies at a Sc concentration a little higher than the average (peak ~ 11 ppm, average = 8.6 ppm), in the range for gabbroic or noritic anorthosite. Textures of several larger, genomict anorthositic rocks collected at the Apollo 16 site (e.g., 60025, 67075) have regions of nearly pure plagioclase and other regions of noritic/gabbroic anorthosite, much as we deduce from the compositional distribution of lithic fragments shown in Fig. 14. Conspicuous by its absence is a peak at ~30 ppm Sc, which would correspond to frozen cotectic melt. This suggests that the bulk of the pyroxene was dispersed among grains and clots of cumulus plagioclase. Had there been a volumetrically significant body of rock or layers more mafic than noritic anorthosite (i.e., plagioclase < 77.5%) as part of the precursor igneous system, there should be a substantial number of samples with Sc concentrations > 15 ppm.

A Common Igneous System

There are reasons to believe the precursor system of FNA composition was a common type of lunar igneous system. On the basis of compositions of highland polymict materials, especially soils, a relatively mafic, ferroan component that is not petrographically obvious and that has a composition not easily matched by known, large lunar igneous rocks seems to be required by mass-balance calculations (e.g., Korotev et al., 1980; Haskin et al., 1981; Korotev, 1981; Stöffler et al., 1981, 1985; Lindstrom and Salpas, 1983; Korotev and Haskin, 1988; Jolliff, 1992b). Lindstrom and Salpas (1983) concluded that fragments of ferroan noritic anorthosite in feldspathic fragmental breccias from North Ray Crater were an essential igneous precursor to the breccias and to certain Apollo 16 melt rocks. McGee (1987) reported on clasts of ferroan noritic anorthosite in 67215 that may represent mafic assemblages related petrogenetically to the more plagioclase-rich ferroan anorthosites (see also Lindstrom and Salpas, 1983; Warren et al., 1990). Relatively mafic clasts of ferroan noritic anorthosite also have been reported in breccia 67016 (Norman, 1981; Norman et al., 1991, 1993; Norman and Taylor, 1992). Indeed, a careful re-evaluation of ferroan-anorthositic-suite rocks and consideration of the bulk composition of the Moon's upper crust led Warren (1990) to conclude that the "overall composition" of the ferroan anorthositic suite must be nearly a factor of two more mafic (but with a large uncertainty) than indicated by the average mode of large ferroan-anorthositic-suite rocks (93–96 vol%, for samples > 10 g, weighted according to mass; Warren, 1990). The FNA system bulk composition, corresponding to ~85 vol% plagioclase, is roughly a factor of two more mafic than the average mode of the large, pristine ferroan-anorthositic-suite samples.

The samples of FNA composition from North Ray Crater and the Antarctic lunar-highland meteorites (e.g., MAC88104/5, Jolliff et al., 1991a; Koeberl et al., 1991; Neal et al., 1991; Warren and Kallemeyn, 1991) are similar in that both contain plagioclase-rich igneous clasts that are relatively mafic compared to most large ferroan-anorthositic-suite samples. On the basis of compositions of melt clasts and bulk samples of the highland meteorites, they appear to contain abundant components whose Sc-Sm and Sc-Al_2O_3 relationships are similar to those of the FNA suite of samples from 67513. Although the incompatible-element concentrations of the FNA suite from 67513 are higher than those of most other ferroan-anorthositic-suite rocks, they are similar to those of many subsamples of the highland meteorites, especially those that have high Sc/Sm (Fig. 15). Many of the subsamples of the lunar-highland meteorites have compositions that lie slightly to the ITE-rich side of the "67513 reference line" on Fig. 15c; we note that some of these are indeed more magnesian or ITE-rich components such as also exist in other lithic fragments of 67513 (cf. Fig. 1a). Nevertheless, the FNA components of these meteorites constitute a substantial proportion such that the bulk composition of MAC88104/5, the most ferroan of the highland meteorites, is very similar to the FNA-system bulk composition as derived herein (see Table 2), and we consider the MAC88105 composition to be fairly representative of the early lunar upper crust, uncontaminated by

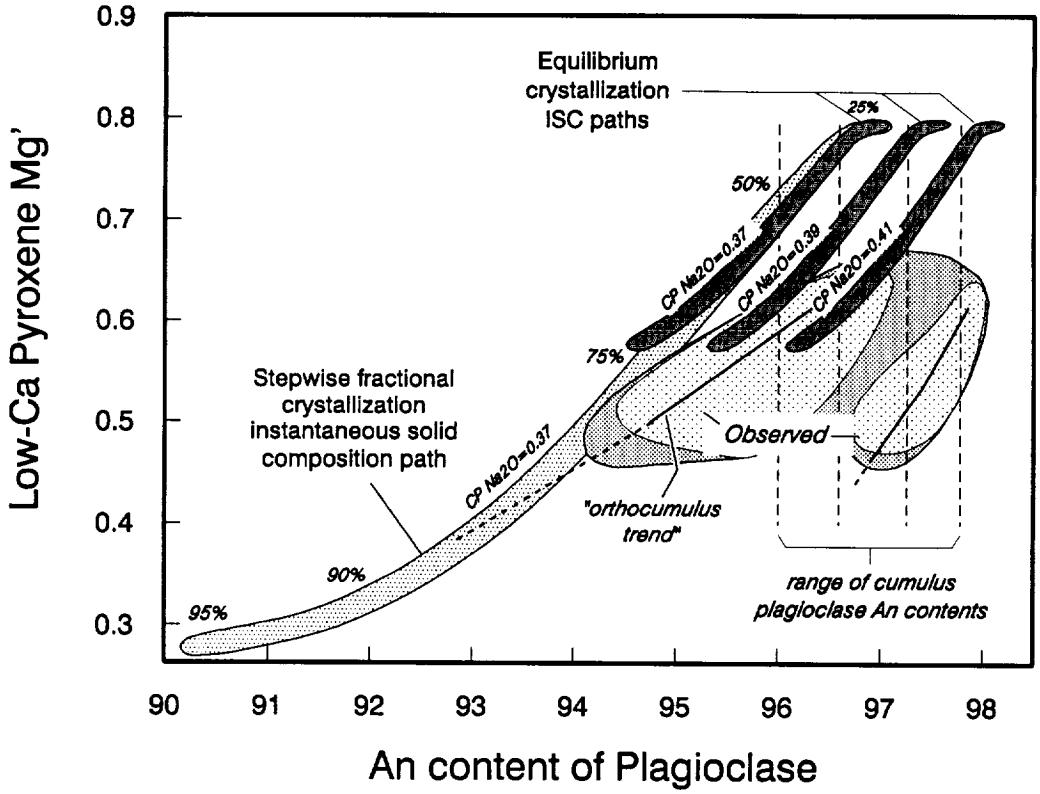

FIG. 13. Mg′ of low-Ca pyroxene vs. An content of plagioclase in model compositions of instantaneous solids (ISC) formed during crystallization of intercumulus melt. Observed compositions of coexisting minerals in fragments from sample 67513 fall within the broad stippled region, mostly within the light stippled areas, suggesting trends as indicated by solid lines. Dashed lines extend these trends to extreme compositions found within a few individual samples. Other samples from Station 11 whose mineral compositions fall within these fields include 67035, 67075, 67215, 67455, 67525, and 67539. Equilibrium crystallization ISC paths are shown for three different intercumulus melt compositions. From mass-balance between 70% cumulus plagioclase and 30% intercumulus melt, we calculated melt compositions corresponding to three different model cumulus-plagioclase compositions with Na_2O concentrations ranging from 0.37 to 0.41 wt%. Dashed lines show the average An contents of observed cumulus-plagioclase compositional clusters (e.g., Fig. 5d). If we select the average Na_2O concentration of the most plagioclase-rich fragments in sample 67513 (0.37 wt%), the ISC mineral compositions are offset only slightly to lower An and higher Mg′ from those observed in the "orthocumulus trend" and they roughly parallel its slope. By taking higher values of Na_2O in model cumulus plagioclase (0.39–0.41), modeled postcumulus-plagioclase compositions bracket the upper part of the "orthocumulus trend." In this case, however, the intercumulus melt would be in equilibrium with plagioclase more calcic than all but the most calcic of the observed cumulus plagioclase. We consider the initial condition corresponding to average cumulus plagioclase Na_2O concentration of 0.37 to be most likely because it is the average observed Na_2O concentration and because the intercumulus melt (0.27% Na_2O by mass balance) is initially in equilibrium with plagioclase of about the same Na_2O concentration as the average (0.37). In purely equilibrium crystallization, mineral compositions evolve no farther than the Mg′ and molar Ca/(Ca + Na + K) of the starting intercumulus-melt composition. Stepwise crystallization effectively isolates early-formed assemblages from later equilibration, allowing mineral compositions to evolve as in fractional crystallization. Percentages adjacent to the stepwise crystallization trend indicate the extent of crystallization of intercumulus melt.

KREEP and mare basalt. If rocks of ferroan noritic-anorthosite composition such as those found at North Ray Crater are more common in the lunar crust than indicated by sampling at other Apollo sites, their abundance may lend further support to their being a specific product of a global magma ocean.

Was the Ferroan Noritic-Anorthosite-Composition Igneous System Formed in a Magma Ocean?

Thus far, we have avoided speculations relating to the origin of the FNA-system parent magma; rather, we have focused on that part of the system preserved in the sample suite from 67513. In this section, we consider the possibility that the FNA system was a product of a magma ocean, and if so, what new insights might be gained on how the magma ocean solidified.

Mineral assemblages, mineral compositions, and bulk incompatible-element concentrations are roughly consistent with formation of the FNA samples after some 75% crystallization of a magma ocean of near-chondritic initial composition. By our estimate, the intercumulus melt associated with cumulus plagioclase at the time of isolation of the system had about 7–9 times chondritic REE concentrations with slight LREE enrichment and a perhaps slightly positive Eu anomaly

Table 5. Stepwise crystallization model compositions.

	"30/70"	25% Cryst'd		50% Cryst'd		75% Cryst'd		90% Cryst'd		95% Cryst'd	
	Cot Mlt	Melt	Solid	Melt	Solid	Melt	Solid	Melt	Solid	Melt	Solid
percent:	100	75	25	50	50	25	75	10	90	5	95
					Oxides (wt.%)						
SiO_2	46.19	47.41	42.60	46.93	48.35	46.00	47.90	44.63	46.89	43.84	46.56
TiO_2	0.60	0.79	0.03	1.16	0.06	2.16	0.12	4.67	0.38	5.76	1.23
Al_2O_3	17.54	14.54	26.38	12.86	17.92	10.78	15.01	9.41	11.75	9.33	11.16
Cr_2O_3	0.23	0.15	0.47	0.13	0.19	0.13	0.14	0.10	0.15	0.10	0.14
FeO	12.83	15.33	5.45	18.31	9.36	22.27	14.21	25.60	19.90	25.57	21.42
MnO	0.20	0.24	0.07	0.29	0.14	0.36	0.22	0.43	0.32	0.43	0.34
MgO	9.53	9.33	10.13	7.46	13.08	4.58	10.45	2.12	6.32	1.72	5.32
CaO	12.50	11.79	14.61	12.34	10.67	12.98	11.68	11.57	13.98	11.09	13.48
Na_2O	0.27	0.27	0.26	0.30	0.22	0.35	0.25	0.43	0.29	0.47	0.32
K_2O	0.053	0.07	0.01	0.10	0.01	0.18	0.02	0.39	0.02	0.71	0.04
P_2O_5	0.050	0.07	0.00	0.10	0.00	0.20	0.00	0.55	0.00	0.98	0.00
					Trace elements (ppm)						
Sc	28	37	2.7	35	39	29	42	18	36	16	32
Cr	1643	1046	3210	909	1321	888	931	701	1020	684	940
Ba	38	50	5.5	72	6	133	9	295	17	530	31
La	2.66	3.52	0.129	5.21	0.132	10.0	0.245	23.2	.71	43.8	1.38
Sm	1.53	2.04	0.039	3.03	0.050	5.74	0.237	12.2	1.17	20.4	1.98
Eu	0.68	0.76	0.45	0.94	0.387	1.37	0.50	2.25	0.76	3.04	0.95
Tb	0.37	0.49	0.006	0.73	0.009	1.37	0.061	2.88	0.31	4.72	0.51
Yb	1.62	2.15	0.028	3.17	0.117	5.80	0.459	11.6	1.72	17.7	2.76
Mg'	0.57	0.52	0.77	0.42	0.71	0.27	0.57	0.13	0.36	0.11	0.31
					Weight fractions of minerals in solid assemblages						
Olivine			0.239		0.056		0.068		0.08		0.045
Plagioclase			0.743		0.51		0.418		0.327		0.308
Pigeonite					0.43		0.397		0.247		0.365
Augite							0.116		0.347 (*)		0.267
Spinel			0.018		0.003						
Ilmenite											0.015
					Mineral component fractions						
Plag An			0.968		0.960		0.944		0.917		0.902
Olivine Fo			0.778		0.701		0.542		0.323		0.279
Pigeonite Mg'					0.720		0.560		0.340		0.300
Augite Mg'							0.620		0.400		0.350

Steps include separation of melt from solid after 25, 50, and 75 percent crystallization at P ~2kb. Compositions at 90 and 95 percent crystallization calculated for 60% and 80%, respectively, equilibrium crystallization of the fourth batch of melt. Starting cotectic (intercumulus) melt composition from Table 2. Derivative melt and solid proportions are given in weight percent. (*) High proportion of augite relative to pigeonite in first half of last 25% crystallization step results from discontinuity on separation of melt and crystals imposed by our model for stepwise crystallization.

(Fig. 8). Moreover, concentrations of Ba, Sr, and REEs in the average FNA cumulus plagioclase composition are within the range estimated by Phinney (1991) for cumulus plagioclase of a hypothetical magma ocean.

The ITE concentrations of the FNA suite, although low compared to average lunar crustal materials, are high relative to many other ferroan-anorthositic-suite samples (e.g., Fig. 15), owing to the intercumulus material. In fact, the composition of intercumulus material corresponds approximately to that of a liquid in equilibrium with the cumulus plagioclase. Thus, using the composition of intercumulus material as the distinguishing criterion (Wadsworth, 1985), these are dominantly orthocumulates, not heteradcumulates or adcumulates bearing rafted mafic cumulus minerals. An orthocumulate with some 17 wt% intercumulus mafic minerals is an alternative to the approximately 17–19 wt% rafted mafic minerals suggested by Warren (1993), on the basis of considerations of density of the magma ocean, plagioclase cumulates, and the bulk crust, and on the basis of mass-balance calculations of the composition of the upper crust. In fact, the lithic fragments in sample 67513 have compositions that we would expect to have been common among products of crystallization in the upper part of a magma ocean.

We suggest two broad constraints on the physical setting where the rocks formed. (1) The FNA system was a plagioclase-rich rock body (~85 vol% plagioclase) that was produced when magma became isolated within a framework of cumulus plagioclase. (2) It was a large body relative to the (unknown) size of the impact(s) that excavated it, because many of the impact-brecciated lithic fragments in sample 67513 consist almost exclusively of FNA components.

For there to have been a large mass of cumulus plagioclase derived from a magma ocean, there must have been an even larger mass of mafic cumulates. In any event, a large mass of plagioclase precipitated from a cotectic liquid would be accompanied by precipitation of a roughly equal mass of mafic minerals, some of which should be combined with plagioclase in relatively mafic rocks. Rocks as mafic as gabbro or norite, however, are not included in any of the FNA polymict (or genomict) impact breccias from 67513, indicating that the scale of the separation of such mafic rocks from cogenetic plagioclase was also large relative to the size of the impactor

that originally excavated these rocks. This is consistent with the concept of a magma ocean, giving perched or near-surface plagioclase-rich rockbergs with attendant intercumulus melt. For example, starting with a magma ocean of 400 km depth and assuming plagioclase saturation after 75% solidification as mafic cumulates that sank or crystallized at the bottom, the upper 83 km would consist of plagioclase-saturated magma and a thin chilled crust. If the upper 83 km of the magma ocean formed a plagioclase orthocumulate, comprising 70 vol% plagioclase and 30 vol% intercumulus material, plus dense, residual gabbronoritic magma and additional mafic cumulates, then the plagioclase orthocumulate would be some 50 km thick, on average. This is easily thick enough to prevent all but the largest basin impacts from penetrating the anorthositic rocks and exhuming any related mafic rocks. Unlike the anorthositic layers of terrestrial mafic intrusions, which are interlayered with mafic rock units, the lunar anorthositic rocks would rise above residual liquids, which on the Moon, follow the trend of Fe enrichment (due to lack of magnetite or amphibole in the crystallization sequence).

There are alternatives to a simple layered magma-ocean origin as outlined above. The two constraints given above require only a large-scale physical separation of mafic rocks from the cumulus-plagioclase–intercumulus-melt system. This might have occurred on the scale of a large pluton, similar in scale to terrestrial massif anorthosites (e.g., see model of Longhi and Ashwal, 1985), which are of sufficient size to host meteorite impacts large enough to generate the range of impactites observed in the rock fragments in sample 67513. The FNA system may have crystallized initially by a process similar to that of the Stillwater thick anorthosites (isolation of cumulus plagioclase and crystallization of intercumulus material), but a second stage involving further separation from mafic rocks and upward migration, as in the origin of terrestrial massif anorthosites, would be required because of the lack of mafic rocks or corresponding mafic impact melts among the impact debris. We note that inclusion-rich plagioclase such as occurs in FNA samples from 67513 is common in massif anorthosites, but not in Stillwater anorthosites. This and the exsolution features observed in pyroxenes support a two-stage petrogenesis for the FNA-composition rocks. Moreover, a two-stage origin such as this would prevent extended communication between intercumulus melt and contemporary magma, leading to a rock body that is mainly orthocumulus rather than adcumulus in nature.

A two-stage origin may have occurred within a crystallizing magma ocean. If the zone of nucleation of plagioclase was deep when plagioclase began to crystallize, the accumulation of plagioclase may have begun at some deep crustal level (i.e., perched) as opposed to migration all the way to the top of the magma (i.e., flotation). Accumulation may have occurred in specifically favorable locations instead of along a broad horizontal zone, thus leading to the formation of plagioclase-rich diapirs within the upper part of the magma ocean. Such diapirs then rose to near the top of the magma ocean, displacing overlying, more dense magma. A more or less continuous process of this kind could lead to a thick pile of noritic-anorthosite plutons in the upper crust, as suggested by Longhi and Ashwal (1985).

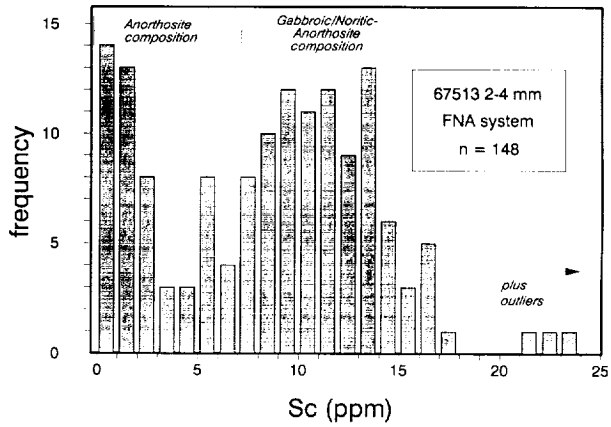

FIG. 14. Histogram of Sc concentrations in FNA-system lithic fragments from sample 67513, showing bimodal distribution. The total number of samples is 148; the average composition of this set is given in Table 2, Col. 2. The mass-weighted mean Sc concentration is 8.63 ppm. Compositional designations of "anorthosite" and "gabbroic/noritic anorthosite" are based on the Sc-Al correlation (Fig. 2).

CONCLUSIONS

We have analyzed a set of rock particles from the rim of North Ray Crater that appears to come from a single igneous system which we refer to as the ferroan noritic-anorthosite composition igneous system. Petrographically and geochemically similar rocks are found as clasts in breccias such as 67455 (Lindstrom and Salpas, 1983) and 67075 (McCallum et al., 1975). The system bulk composition inferred from lithic fragments of sample 67513 is that of ferroan noritic anorthosite, with ~30 wt% Al_2O_3 and Mg′ of 0.56. Most of the 2–4 mm particles are polymict (dominantly genomict) breccias, but many contain relict igneous clasts. A much smaller number of fragments are entirely monomict and retain relicts of their original igneous texture. Many have the composition of anorthosite, but most have the composition and mineralogy of noritic or gabbroic anorthosite. A few are anorthositic gabbro or anorthositic norite. The compositional distribution of fragments is that expected for a plagioclase-rich body with relatively small-scale (centimeter to decimeter) segregations of plagioclase and anorthositic norite, not a massively layered system of anorthosite and gabbro or norite.

Mineral compositions and geochemical characteristics suggest that these rocks formed as a cotectic mafic liquid crystallized within a framework of cumulus plagioclase. The mass balance for this "system" was ~70 wt% cumulus plagioclase and 30 wt% intercumulus, cotectic melt. The system originated as a perched or suspension cumulate, which evolved to a point where through-flow or exchange of contemporary magma was restricted, leading to an orthocumulate with a total of ~85 vol% plagioclase. The intercumulus melt solidified (postcumulus stage) mainly by equilibrium crystallization, but with minor, localized, late-stage fractional crystallization and migration of residual liquid.

These processes can produce most of the range of bulk compositions, mineral compositions, and mineral assemblages, including the inferred order of crystallization; how-

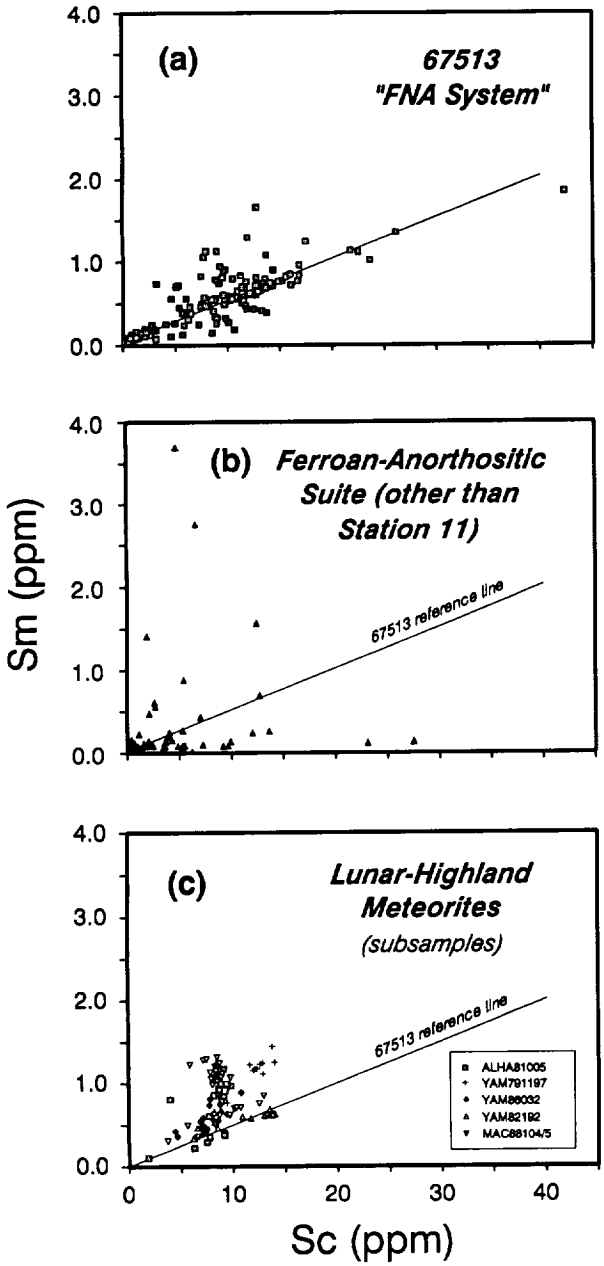

FIG. 15. Concentrations of Sc vs. Sm comparing (a) samples of the FNA suite from 67513, (b) samples of the ferroan anorthositic suite from locations other than North Ray Crater, including other Apollo sites, and (c) subsamples of the lunar-highland meteorites collected in Antarctica. Data sources include Hubbard et al., 1974; Wänke et al., 1974; Warren and Wasson, 1978; Blanchard and Budahn, 1979; Haskin et al., 1981; Korotev et al., 1983; Warren et al., 1983a,b, 1986, 1987, 1991; Ryder and Norman, 1980; Ryder, 1985; Lindstrom et al., 1986; Salpas et al., 1988; James et al., 1989, 1991; Jolliff et al., 1991a,b; Laul et al., 1989.

ever, they do not by themselves produce the full range of observed geochemical and petrographic characteristics. Some recrystallization of cumulus plagioclase and exchange of components between cumulus plagioclase and intercumulus materials is indicated. Observed mineral compositions, for example, the high and restricted range of plagioclase An contents and complex compositional zoning patterns of plagioclase, are consistent with partial reaction or reequilibration between intercumulus minerals or melt and a portion of the cumulus plagioclase, possibly aided by recrystallization.

A two-stage genesis is indicated for these rocks. The first stage of formation is roughly analogous to that of anorthosites of the Middle Banded Zone of the terrestrial Stillwater Complex. The rocks derive from a system of accumulated plagioclase and entrained intercumulus melt in which cumulus plagioclase had previously separated from cogenetic mafic minerals. Unlike the Stillwater anorthosites, however, there was no significant communication between the intercumulus melt and a larger reservoir of similar melt, leading to a predominantly orthocumulus rather than adcumulus rock system for the lunar rocks. The overall igneous system was large enough that later meteorite impacts that produced FNA-composition breccias did not sample mafic cumulates that might have been cogenetic with cumulus plagioclase. Thus, either the plagioclase cumulate was extremely thick, as in the case of a deep magma ocean, or the second stage involved extensive further separation from related mafic rocks, which may have occurred when the plagioclase-rich cumulate system became diapirically buoyant and separated from (or moved to the top of) the larger magma system. A two-stage origin such as this may provide the driving force for recrystallization and reequilibration indicated by our geochemical model. Thus, the second stage of formation of these rocks, which may be analogous to the formation of terrestrial massif anorthosites, involved diapiric rise of the system to an upper crustal level, whether from a discrete magma at the base of the crust or from a deep plagioclase accumulation in a magma ocean.

Acknowledgments—This work was funded by NASA Grants NAG 9-56 and NAGW-3343 to L. A. Haskin. We thank Randy Korotev for his hard work in reducing INAA data and for many late-night sample changes. We thank John Longhi for the use of his computer programs MAGFOX and MAGPOX. Careful reviews of the manuscript by Gordon McKay, Chip Shearer, and Greg Snyder, and of an earlier version of the manuscript by Odette James, Randy Korotev, John Longhi, and Paul Warren, led to significant improvements and are appreciated.

Editorial handling: J. N. Grossman

REFERENCES

Albee A. L., Quick J. E., and Chodos A. A. (1977) Source and magnitude of errors in "broad-beam analysis" (DBA) with the electron probe. *Lunar Sci. VIII*, 7–9 (abstr.).

Beattie P. et al. (1993) Terminology for trace element partitioning. *Geochim. Cosmochim. Acta* **57**, 1605–1606.

Bence A. E. and Albee A. L. (1968) Empirical correction factors for the electron microanalysis of silicates and oxides. *J. Geol.* **76**, 382–403.

Blanchard D. P. and Budahn J. R. (1979) Remnants from the ancient lunar crust: Clasts from consortium breccia 73255. *Proc. 10th Lunar Sci. Conf.*, 803–816.

Blundy J. D. and Wood B. J. (1991) Crystal-chemical controls on the partitioning of Sr and Ba between plagioclase feldspar, silicate melts, and hydrothermal solutions. *Geochim. Cosmochim. Acta* **55**, 193–209.

Brown R. W. (1977) A sample fusion technique for whole rock analysis with the electron microprobe. *Geochim. Cosmochim. Acta* **41**, 435–438.

Dixon J. R. and Papike J. J. (1975) Petrology of anorthosites from the Descartes region of the moon: Apollo 16. *Proc. 6th Lunar Sci. Conf.*, 263–291.

Drake M. J. and Weill D. F. (1975) Partition of Sr, Ba, Ca, Y, Eu^{2+}, Eu^{3+}, and other REE between plagioclase feldspar and magmatic liquid: An experimental study. *Geochim. Cosmochim. Acta* **39**, 689–712.

Gill J. B. (1979) Role of trace element partition coefficients in models of andesite genesis. *Geochim. Cosmochim. Acta* **42**, 709–724.

Gitlin E. C., Salpas P. A., McCallum I. S., and Haskin L. A. (1985) Small scale compositional heterogeneities in Stillwater anorthosite II. *Lunar Planet. Sci. XVI*, 272–273 (abstr.).

Gladney E. S. and Roelandts I. (1988) 1987 compilation of elemental concentration data for USGS BHVO-1, MAG-1, QLO-1, RGM-1, Sco-1, SDC-1, SGR-1, and STM-1. *Geostand. Newslett.* **12**, 253–362.

Govindaraju K. and Roelandts I. (1993) Second report (1993) on the first three GIT-IWG rock reference samples: Anorthosite from Greenland, AN-G; Basalte d'Essey-la-Côte, BE-N; Granite de Beauvoir, MA-N. *Geostand. Newslett.* **17**, 227–294.

Haskin L. A. (1984) Petrogenetic modeling—The use of rare earth elements. In *Developments in Geochemistry 2: Rare Earth Element Geochemistry* (ed. P. Henderson), pp. 115–152. Elsevier.

Haskin L. A. and Lindstrom D. J. (1988) On identifying parent plutonic rocks from lunar breccia and soil fragments. *Proc. 18th Lunar Planet Sci. Conf.*, 1–9.

Haskin L. A. and Salpas P. A. (1992) Genesis of compositional characteristics of Stillwater AN-I and AN-II thick anorthosite units. *Geochim. Cosmochim. Acta* **56**, 1187–1212.

Haskin L. A., Lindstrom M. M., Salpas P. A., and Lindstrom D. J. (1981) On compositional variations among lunar anorthosites. *Proc. Lunar Planet. Sci. 12B*, 41–66.

Hawke B. R., Lucey P. G., and Taylor G. J. (1992) The distribution of anorthosite on the nearside of the Moon. In *Workshop on the Physics and Chemistry of Magma Oceans from 1 bar to 4 Mbar*, pp. 20–21. LPI.

Hubbard N. J., Rhodes M. J., Wiesmann H., Shih C.-Y., and Bansal B. M. (1974) The chemical definition and interpretation of rock types returned from the non-mare regions of the Moon. *Proc. 5th Lunar Sci. Conf.*, 1227–1246.

Irving A. J., Merrill R. B., and Singleton D. E. (1978) Experimental partitioning or rare earth elements and scandium among armalcolite, ilmenite, olivine, and mare basalt liquid. *Proc. 9th Lunar Planet. Sci. Conf.*, 601–612.

James O. B. (1980) Rocks of the early lunar crust. *Proc. 11th Lunar Planet. Sci. Conf.*, 365–393.

James O. B. (1988) Trace elements in the plagioclase of lunar ferroan anorthosites. *Lunar Planet. Sci. XIX*, 547–548 (abstr.).

James O. B., Lindstrom M. M., and Flohr M. K. (1987) Petrology and geochemistry of alkali gabbronorites from lunar breccia 67975. *Proc. 17th Lunar Planet Sci. Conf.; J. Geophys. Res.*, **92** (Suppl.), E314–E330.

James O. B., Lindstrom M. M., and Flohr M. K. (1989) Ferroan anorthosite from lunar breccia 64435: Implications for the origin and history of lunar ferroan anorthosites. *Proc. 19th Lunar Planet. Sci. Conf.*, 219–243.

James O. B., Lindstrom M. M., and McGee J. J. (1991) Lunar ferroan anorthosite 60025: Petrology and chemistry of mafic lithologies. *Proc. Lunar Planet. Sci.* **21**, 63–87.

Jolliff B. L. (1991) Compositional variations of particles from North Ray Crater soil 67513 and implications for the composition of the lunar highlands. *Lunar Planet. Sci. XXII*, 653–654 (abstr.).

Jolliff B. L. (1992a) A new angle on lunar ferroan-suite differentiation. In *Workshop on the Physics and Chemistry of Magma Oceans from 1 bar to 4 Mbar*, pp. 18–19. LPI.

Jolliff B. L. (1992b) Mafic, ferroan lithologies from North Ray Crater, Apollo 16: Implications for crustal abundance. *Lunar Planet. Sci. XXIII*, 623–624 (abstr.).

Jolliff B. L., Korotev R. L., and Haskin L. A. (1991a) A ferroan region of the lunar highlands as recorded in meteorites MAC88104 and MAC88105. *Geochim. Cosmochim. Acta* **55**, 3051–3071.

Jolliff B. L., Korotev R. L., and Haskin L. A. (1991b) Geochemistry of 2–4 mm particles from Apollo 14 soil (14161) and implications regarding igneous components and soil-forming processes. *Proc. Lunar Planet. Sci.*, **21**, 193–219.

Koeberl C., Kurat G., and Brandstätter F. (1991) MAC88105—A regolith breccia from the lunar highlands: Mineralogical, petrological, and geochemical studies. *Geochim. Cosmochim. Acta* **55**, 3073–3087.

Korotev R. L. (1981) Compositional trends in Apollo 16 soils. *Proc. 12th Lunar Planet Sci. Conf.*, 577–605.

Korotev R. L. (1982) Comparative geochemistry of Apollo 16 surface soils and samples from cores 64002 and 60002 through 60007. *Proc. 13th Lunar Planet. Sci. Conf.; J. Geophys. Res.* **87**, A269–A278.

Korotev R. L. (1991) Geochemical stratigraphy of two regolith cores from the central highlands of the Moon. *Proc. Lunar Planet. Sci.* **21**, 229–289.

Korotev R. L. (1994) Compositional variation in Apollo 16 impact-melt breccias and inferences for the geology and bombardment history of the Central Highlands of the Moon. *Geochim. Cosmochim. Acta* **58**, 3931–3969.

Korotev R. L. and Haskin L. A. (1988) Europium mass balance in polymict samples and implications for plutonic rocks of the lunar crust. *Geochim. Cosmochim. Acta* **52**, 1795–1813.

Korotev R. L., Haskin L. A., and Lindstrom M. M. (1980) A synthesis of lunar highlands compositional data. in *Proc. 11th Lunar Planet. Sci. Conf.*, 395–429.

Korotev R. L., Lindstrom M. M., Lindstrom D. J., and Haskin L. A. (1983) Antarctic meteorite ALHA81005—Not just another lunar noritic anorthosite. *Geophys. Res. Lett.* **10**, 829–832.

Laul J. C., Gosselin D. C., Galbreath K. C., Simon S. B., and Papike J. J. (1989) Chemistry and petrology of Apollo 17 highland coarse fines: Plutonic and melt rocks. *Proc. 19th Lunar Planet. Sci. Conf.*, 85–97.

Lindsley D. H. and Andersen D. J. (1983) A two-pyroxene thermometer. *Proc. 13th Lunar Planet. Sci. Conf.; J. Geophys. Res.* **88**, A887–A906.

Lindstrom D. J. (1976) Experimental study of the partitioning of the transition metals between clinopyroxene and coexisting liquids. Ph.D. thesis, Univ. Oregon.

Lindstrom D. J. and Korotev R. L. (1982) TEABAGS: Computer programs for instrumental neutron activation analysis. *J. Radioanal. Nucl. Chem.* **70**, 439–458.

Lindstrom M. M. and Salpas P. (1981) Geochemical studies of rocks from North Ray Crater, Apollo 16. *Proc. Lunar Planet. Sci. Conf. 12B*, 305–322.

Lindstrom M. M. and Salpas P. (1983) Geochemical studies of feldspathic fragmental breccias and the nature of North Ray Crater ejecta. *Proc. 13th Lunar Planet. Sci. Conf.; J. Geophys. Res.* **88**, A671–A683.

Lindstrom M. M., Lindstrom D. J., Korotev R. L., and Haskin L. A. (1986) Lunar meteorite YAMATO-791197: A polymict anorthositic norite breccia. In *Proceedings of the Tenth Symp. Antarctic Meteorites, NIPR Spec Iss.* **41**, 58–75.

Longhi J. (1977) Magma oceanography 2: Chemical evolution and crustal formation. *Proc. 8th Lunar Sci. Conf.*, 601–621.

Longhi J. (1978) Pyroxene stability and the composition of the lunar magma ocean. *Proc. 9th Lunar Planet. Sci. Conf.*, 285–306.

Longhi J. (1980) A model of early lunar differentiation. *Proc. 11th Lunar Planet. Sci. Conf.*, 289–315.

Longhi J. (1987) Liquidus equilibria and solid solution in the system $CaAl_2Si_2O_8$-Mg_2SiO_4-$CaSiO_3$-SiO_2 at low pressure. *Amer. J. Sci.* **287**, 265–331.

Longhi J. (1991) Comparative liquidus equilibria of hypersthene-normative basalts at low pressure. *Amer. Mineral.* **76**, 785–800.

Longhi J. and Ashwal L. D. (1985) Two-stage models for lunar and terrestrial anorthosites: Petrogenesis without a magma ocean. *Proc. 15th Lunar Planet. Sci. Conf.; J. Geophys. Res.* **90**, C571–C584.

Longhi J. and Boudreau A. E. (1979) Complex igneous processes and the formation of the primitive lunar crustal rocks. *Proc. 10th Lunar Planet. Sci. Conf.*, 2085–2105.

Longhi J., Walker D., and Hays J. F. (1976) Fe and Mg in plagioclase. *Proc. 7th Lunar Sci. Conf.*, 1281–1300.

Marsh B. D. and Maxey M. R. (1985) On the distribution and separation of crystals in a convecting magma. *J. Volcanol. Geotherm. Res.* **24,** 95–150.

Marvin U. B. (1972) *Apollo 16 coarse fines (4–10 mm): Sample Classification, Description and Inventory.* NASA Catalog.

Marvin U. B., Lindstrom M. M., Bernatowicz T. J., Podosek F. A., and Sugiura N. (1987) The composition and history of breccia 67015 from North Ray Crater. *Proc. 17th Lunar Planet. Sci. Conf.; J. Geophys. Res.* **92,** E471–E490.

McCallum I. S., Okamura F. P., and Ghose S. (1975) Mineralogy and petrology of sample 67075 and the origin of lunar anorthosites. *Earth Planet. Sci. Lett.* **26,** 36–53.

McCallum I. S., Raedeke L. D., and Mathez E. A. (1980) Investigations of the Stillwater Complex: Part I. Stratigraphy of the structure of the banded zone. *Amer. J. Sci.* **280A,** 59–87.

McGee J. J. (1987) Petrology of brecciated ferroan noritic anorthosite 67215. *Proc. 18th Lunar Planet. Sci. Conf.*, 21–31.

McGee J. J. (1993) Lunar ferroan anorthosites: Mineralogy, compositional variations, and petrogenesis. *J. Geophys. Res.* **98,** 9089–9105.

McGee J. J. (1994) Lunar ferroan anorthosite subgroups. *Lunar Planet. Sci. XXV*, 875–876 (abstr.).

McKay G. A. (1982) Partitioning of REE between olivine, plagioclase, and synthetic melts: Implications for the origin of lunar anorthosite. *Lunar Planet. Sci. XIII*, 493–494 (abstr.).

McKay G. A. (1986) Crystal/liquid partitioning of REE in basaltic systems: Extreme fractionation of REE in olivine. *Geochim. Cosmochim. Acta* **50,** 69–79.

McKay G. A. and Weill D. F. (1976) Petrogenesis of KREEP. *Proc. 7th Lunar Sci. Conf.*, 2427–2447.

McKay G. A. and Weill D. F. (1977) KREEP petrogenesis revisited. *Proc. 8th Lunar Sci. Conf.*, 2339–2355.

McKay G., Wagstaff J., and Yang S.-R. (1986) Clinopyroxene REE distribution coefficients for shergottites: The REE content of the Shergotty melt. *Geochim. Cosmochim. Acta* **50,** 927–937.

McKay G., Wagstaff J., and Le L. (1990) REE distribution coefficients for pigeonite: Constraints on the origin of the mare basalt europium anomaly. In *Workshop on Lunar Volcanic Glasses: Scientific and Resource Potential* (ed. J. W. Delano and G. H. Heiken); LPI Tech. Rpt. 90-02, pp. 48–49. LPI.

Minkin J. A., Thompson C. L., and Chao E. C. T. (1977) Apollo 16 white boulder consortium samples 67455 and 67475: Petrologic investigation. *Proc. 8th Lunar Sci. Conf.*, 1967–1986.

Morris R. V., Score R., Dardano C., and Heiken G. (1983) *Handbook of Lunar Soils, Part II: Apollo 16–17; NASA Publication 67*, pp. 578–615.

Morrison D. A., Phinney W. C., and Maczuga D. E. (1987) Archean anorthosites: Constraints on the accumulation process. *Lunar Planet. Sci. XVIII*, 670–671 (abstr.).

Morse S. A. (1982) Adcumulus growth of anorthosite at the base of the lunar crust. *Proc. 13th Lunar Planet. Sci. Conf.; J. Geophys. Res.* **87,** A10–A18.

Morse S. A. (1984) Cation diffusion in plagioclase feldspar. *Science* **225,** 504–505.

Nazarov M. A., Ignatenko K. I., and Shevaleevsky I. D. (1982) Source of errors in defocussed beam analysis with the electron probe, revisited. *Lunar Planet. Sci. XIII*, 582–583 (abstr.).

Neal C. R., Taylor L. A., Lui Y., and Schmitt R. A. (1991) Paired lunar meteorites MAC88104 and MAC88105: A new "FAN" of lunar petrology. *Geochim. Cosmochim. Acta* **55,** 3037–3049.

Nord G. L., Jr. (1976) 76535: Thermal history deduced from pyroxene precipitation in anorthite. *Proc. 7th Lunar Sci. Conf.*, 1875–1888.

Norman M. D. (1981) Petrology of suevitic lunar breccia 67016. *Proc. Lunar Planet. Sci. 12B*, 235–252.

Norman M. D. and Ryder G. (1980) Geochemical constraints on the igneous evolution of the lunar crust. *Proc. 11th Lunar Planet. Sci. Conf.*, 317–331.

Norman M. D. and Taylor S. R. (1992) Geochemistry of plutonic anorthosites from Apollo 16 breccia 67016: Lunar crustal evolution and the composition of the Moon. *Geochim. Cosmochim. Acta* **56,** 1013–1024.

Norman M. D., Taylor G. J., and Keil K. (1991) Additional complexity in the lunar crust: Petrology of sodic anorthosites and sulfur-rich, ferroan noritic anorthosites. *Geophys. Res. Lett.* **18,** 2081–2084.

Norman M. D., Alibert C., and McCulloch M. T. (1993) Fragments of ancient lunar crust: Ferroan noritic anorthosites from the Descartes region of the Moon. *Lunar Planet. Sci. XXIV*, 1089–1090 (abstr.).

Papike J. J., Taylor L. A., and Simon S. B. (1991) Lunar Minerals. In *Lunar Sourcebook, A User's Guide to the Moon* (ed. G. Heiken, D. Vaniman, and B. M. French), pp. 121–181. Cambridge Univ. Press.

Peckett A. and Brown G. A. (1973) Plutonic or metamorphic equilibration in Apollo 16 lunar pyroxenes. *Nature* **242,** 252–255.

Phinney W. C. (1991) Lunar anorthosites, their equilibrium melts and the bulk Moon. *Proc. Lunar Planet. Sci.* **21,** 29–49.

Phinney W. C. (1992) Partition coefficients for iron between plagioclase and basalt as a function of oxygen fugacity: Implications for Archean and lunar anorthosites. *Geochim. Cosmochim. Acta* **56,** 1885–1895.

Phinney W. C. (1994) FeO and MgO in plagioclase of lunar anorthosites: Igneous or metamorphic? *Lunar Planet. Sci. XXV*, 1081–1082 (abstr.).

Phinney W. C. and Morrison D. A. (1990) Partition coefficients for calcic plagioclase: Implications for Archean anorthosites. *Geochim. Cosmochim. Acta* **54,** 1639–1654.

Raedeke L. D. and McCallum I. S. (1980) A comparison of fractionation trends in the lunar crust and the Stillwater Complex. In *Proc. Conf. Lunar Highlands Crust* (ed. J. J. Papike and R. B. Merrill), pp. 133–153.

Ryder G. (1982) Lunar anorthosite 60025, the petrogenesis of lunar anorthosites, and the composition of the Moon. *Geochim. Cosmochim. Acta* **46,** 1591–1601.

Ryder G. (1985) *Catalog of Apollo 15 Rocks.* Curatorial Publication 20787. NASA Johnson Space Center, Houston, Texas.

Ryder G. (1992) Chemical variation and zoning of olivine in lunar dunite 72415: Near-surface accumulation. *Proc. Lunar Planet. Sci.* **22,** 373–380.

Ryder G. and Norman M. (1979) *Catalog of Pristine Non-Mare Materials*, rev. ed.; *NASA Curatorial Branch Publication No. 14565.*

Ryder G. and Norman M. (1980) *Catalog of Apollo 16 Rocks; NASA Curatorial Branch Publication No. 16904.*

Salpas P. A., Haskin L. A., and McCallum I. S. (1983) Stillwater anorthosites: A lunar analog? *Proc. 14th Lunar Planet. Sci. Conf.; J. Geophys. Res.* **88** (Suppl.), B27–B39.

Salpas P. A., Lindstrom M. M., and Taylor L. A. (1988) Highland materials at Apollo 17: Contributions from 72275. *Proc. 18th Lunar Planet. Sci. Conf.*, 11–19.

Smith J. V. and Brown W. L. (1988) *Feldspar Minerals, Volume 1, Crystal Structures, Physical, Chemical, and Microtextural Properties*, 2nd ed. Springer-Verlag.

Smith J. V. and Steele I. M. (1974) Intergrowths in lunar and terrestrial anorthosites with implications for lunar differentiation. *Amer. Mineral.* **59,** 673–680.

Snyder G. A., Taylor L. A., and Neal C. R. (1992) A chemical model for generating the sources of mare basalts: Combined equilibrium and fractional crystallization of the lunar magmasphere. *Geochim. Cosmochim. Acta* **56,** 3809–3823.

Stewart D. B. (1975) Apollonian metamorphic rocks—The products of prolonged subsolidus equilibration. *Lunar Science VI*, 774–776 (abstr.).

Stöffler D., Knöll H.-D., Marvin U. B., Simonds C. H., and Warren P. H. (1980) Recommended classification and nomenclature of lunar highland rocks—a committee report. In *Proc. Conf. Lunar*

Highlands Crust (ed. J. J. Papike and R. B. Merrill); *Geochim. Cosmochim. Acta* (Supplement 12), 51–70.
Stöffler D., Ostertag R., Reimold W. U., Borchardt R., Malley J., and Rehfeldt A. (1981) Distribution and provenance of lunar highland rock types at North Ray Crater, Apollo 16. *Proc. Lunar Planet. Sci. 12B*, 185–207.
Stöffler D. et al. (1985) Composition and evolution of the lunar crust in the Descartes Highlands. *Proc. 15th Lunar Planet. Sci. Conf.; J. Geophys. Res.* **90**, C449–C506.
Ulrich G. E. (1981) Geology of North Ray Crater. In *Geology of the Apollo 16 Area, Central Lunar Highlands; USGS Prof. Paper 1048*, pp. 45–81.
Wadsworth W. J. (1985) Terminology of postcumulus processes and products in the Rhum layered intrusion. *Geol. Mag.* **122**, 549–554.
Wager L. R., Brown G. M., and Wadsworth W. J. (1960) Types of igneous cumulates. *J. Petrol.* **1**, 73–85.
Walker D. (1983) Lunar and terrestrial crust formation. *Proc. 14th Lunar Planet Sci. Conf.; J. Geophys. Res.* **88**, B17–B25.
Walker D., Longhi J., Grove T. L., Stolper E., and Hays J. F. (1973) Experimental petrology and origin of rocks from the Descartes Highlands. *Proc. 4th Lunar Sci. Conf.*, 1013–1032.
Wänke H. et al. (1974) Chemistry of Apollo 16 and 17 samples: Bulk composition, late stage accumulation and early differentiation of the Moon. *Proc. 5th Lunar Sci. Conf.*, 1307–1335.
Wänke H. et al. (1975) New data on the chemistry of lunar samples: Primary matter in the lunar highlands and the bulk composition of the Moon. *Proc. 6th Lunar Sci. Conf.*, 1313–1340.
Warren P. H. (1990) Lunar anorthosites and the magma-ocean plagioclase-flotation hypothesis: Importance of FeO enrichment in the parent magma. *Amer. Mineral.* **75**, 46–58.
Warren P. H. (1993) A concise compilation of petrologic information on possibly pristine nonmare Moon rocks. *Amer. Mineral.* **78**, 360–376.
Warren P. H. and Kallemeyn G. W. (1991) The MacAlpine Hills lunar meteorite and implications of the lunar meteorites collectively for the composition and origin of the Moon. *Geochim. Cosmochim. Acta* **55**, 3123–3138.
Warren P. H. and Wasson J. T. (1978) Compositional-petrographic investigation of pristine nonmare rocks. *Proc. 9th Lunar Planet. Sci. Conf.*, 185–217.
Warren P. H., Taylor G. J., Keil K., Kallemeyn G. W., Rosener P. S., and Wasson J. T. (1983a) Sixth Foray for pristine nonmare rocks and an assessment of the diversity of lunar anorthosites. *Proc. 13th Lunar Planet. Sci. Conf.; J. Geophys. Res.* **88**, A615–A630.
Warren P. H., Taylor G. J., Keil K., Kallemeyn G. W., Shirley D. N., and Wasson J. T. (1983b) Seventh Foray: Whitlockite-rich lithologies, a diopside-bearing troctolitic anorthosite, ferroan anorthosites, and KREEP. *Proc. 14th Lunar Planet. Sci. Conf.; J. Geophys. Res.* **88**, B151–B164.
Warren P. H., Shirley D. N., and Kallemeyn G. W. (1986) A potpourri of pristine Moon rocks, including a VHK mare basalt and a unique, augite-rich Apollo 17 anorthosite. *Proc. 16th Lunar Planet. Sci. Conf.; J. Geophys. Res.* **91**, D319–D330.
Warren P. H., Jerde E. A., and Kallemeyn G. W. (1987) Pristine Moon rocks: A "large" felsite and a metal-rich ferroan anorthosite. *Proc. 17th Lunar Planet. Sci. Conf.; J. Geophys. Res.* **92**, E303–E313.
Warren P. H., Jerde E. A., and Kallemeyn G. W. (1990) Pristine Moon rocks: An alkali anorthosite with coarse augite exsolution from plagioclase, a magnesian harzburgite, and other oddities. *Proc. 20th Lunar Planet. Sci. Conf.*, 31–59.
Warren P. H., Jerde E. A., and Kallemeyn G. W. (1991) Pristine Moon rocks: Apollo 17 anorthosites. *Proc. Lunar Planet. Sci.* **21**, 31–59.
Weaver B. L., Tarney J., and Windley B. (1981) Geochemistry and petrogenesis of the Fiskenaesett anorthosite complex, southern Greenland: Nature of the parent magma. *Geochim. Cosmochim. Acta* **45**, 711–725.
Weill D. F. and McKay G. A. (1975) The partitioning of Mg, Fe, Sr, Ce, Sm, Eu, and Yb in lunar igneous systems and a possible origin of KREEP by equilibrium partial melting. *Proc. 6th Lunar Sci. Conf.*, 1143–1158.

APPENDIX

The lithic fragments described below are from sample 67513, collected from the southeastern rim of North Ray Crater, within a few meters of the white-breccia boulders at Station 11 (Fig. A1). Sample 67513 is the 2–4 mm sieved split (19.4 g) of 67510 (originally 134 g). We selected this sample for detailed analysis partly because the <1 mm fine split, 67511, has compositional characteristics more like those of ferroan-anorthositic-suite igneous rocks than does any other Apollo 16 soil. These characteristics include relatively low Mg′, ~0.64 low concentrations of incompatible trace elements (ITE); and high bulk Sc/Sm (Korotev, 1982; Morris et al., 1983). This soil, taken as part of a rake sample, is immature (I_s/FeO = 8.8, Morris et al., 1983), suggesting that it has not been reworked extensively by surface processes. Macroscopic descriptions of the 4–10 mm lithic fragments suggest that, in addition to polymict breccias, the sample contains plagioclase-rich igneous fragments, including gabbroic anorthosite (Marvin, 1972).

Description of Individual Monomict Igneous Samples

67513,7012—Pyroxene-rich ferroan gabbronorite

This sample, originally 41 mg, consists of calcic plagioclase (~An_{95}), finely exsolved, ferroan pyroxenes, ilmenite, disseminated troilite, and Cr-spinel included in pyroxene (Table A1, Fig. A2a,b). The overall texture is cataclastic from moderate shock deformation, but relict, relatively coarse grains reflect a hypidiomorphic-granular original texture.

Aggregates of fractured plagioclase grains constitute remnants of originally blocky grains ranging in size up to 1.2 mm. These generally have undulatory extinction and cataclastic texture, but some grains retain lath shapes. Many of the coarse plagioclase grains contain abundant, evenly distributed mafic granules, generally 1–2 μm or smaller in size. Qualitative analyses by energy-dispersive electron-microprobe and laser-Raman-microprobe techniques indicate that these are Ca-rich pyroxene. In several grains, mafic granules are oriented along parallel planes within the host plagioclase. Coarse plagioclase grains have core compositions ranging from $An_{94.5}$ to $An_{96.5}$, and some have very thin, relatively sodic rims (~An_{93-94}) where they

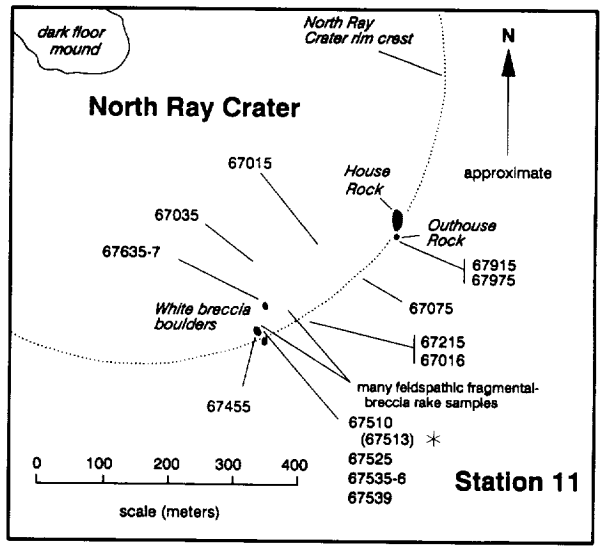

FIG. A1. Planimetric map of Station 11 sampling site at the rim of North Ray Crater, Apollo 16 landing site, after Ulrich (1981). Locations are shown for samples discussed in the text.

Table A1. Mineral modes (volume percent) of representative monomict ferroan noritic-anorthosite-system lithic fragments from sample 67513.

sample No.	,7012	,7052	,7061	,7071	,7075	,7097
mass	40.5	39.8	26.8	24.6	16.2	18.2
Plagioclase	33.8	93.7	87.0	99.7	95.3	59.7
Low-Ca Pyroxene	44.7	4.5	9.6	0.1	3.4	31.3
High-Ca Pyroxene	20.8	1.7	3.3	0.2	1.3	8.7
Sum Pyroxene	65.5	6.3	12.9	0.3	4.7	40.0
Olivine		0.01			0.01	
Ilmenite	0.3		0.06			0.13
Cr-Spinel	0.2	0.03	0.03		0.01	0.10
troilite	0.07					0.06
Assemblages:	,7012 - gabbronorite			,7071 - anorthosite		
	,7052 - anorthosite			,7075 - anorthosite breccia		
	,7061 - noritic anorthosite			,7097 - gabbronorite		

contact pyroxene. Compositions of fine-grained, interstitial plagioclase extend to $\sim An_{90}$ (Table A2).

Pyroxene grains range up to 1.2 mm in size and contain very fine exsolution lamellae (mostly <5 μm). Clinopyroxene grains that have intermediate bulk Ca concentrations (Wo_{21}, $Mg' = 0.54$, Table A3) and that have subequal proportions of exsolved augite and pigeonite, form cores up to several hundred micrometers in maximum dimension that are mantled by inverted pigeonite. Cores appear to have been partially resorbed prior to overgrowth. It is unclear whether the clinopyroxene cores crystallized initially as subcalcic augite or very calcic pigeonite, but it appears that, after exsolution, the host is high-Ca pyroxene (Fig. A2b). Inverted pigeonite (bulk composition Wo_{12}, $Mg' = 0.53$) contains irregularly distributed augite lamellae up to ~ 10 μm thick. Augite grains (Wo_{39}, $Mg' = 0.63$) contain low-Ca pyroxene lamellae. Bulk compositions of early-formed clinopyroxenes (presumably C2/c) of intermediate Ca concentrations indicate a crystallization temperature of about 1175°C (Lindsley and Andersen (1983) geothermometer) followed by later crystallization of pigeonite ($P2_1/c$?) and augite 50 to 80° lower, and exsolution to about 800°C (Fig. A3a, Table A3).

Ilmenite poor in Mg (MgO = 1.3%) occurs as discrete grains up to 400 μm across, as well as 1–10 μm exsolved grains in pyroxene. Pyroxenes also contain very fine-grained inclusions (exsolved ?) of Cr-spinel ($Chr_{62}Ple_{20}Ulv_{18}$). Elongate, submicron inclusions are oriented along crystallographic axes, whereas coarser spinel grains lie along fracture surfaces, and in some cases, appear to outline relict crystal faces. The fine-grained oxide inclusions give host pyroxenes a dark appearance under the petrographic microscope. In fact, bulk subcalcic-augite cores are richer in Fe, relative to their Wo content, and much richer in Cr than the sum of their individual pyroxene exsolution lamellae, reflecting the abundance of Cr-spinel inclusions.

Sample 67513,7012 shows a range of deformation features; some grains have microfault (sheared) offsets, and the thin section contains a 400 μm shear zone within which mineral grains are strongly cataclasized (Fig. A2a). The pyroxenes in this sample are similar in texture and composition to those described from 67075 anorthositic fragmental breccia by McCallum et al. (1975).

67513,7097—Ferroan gabbronorite

This 18-mg sample comprises some 60 vol% plagioclase and 40% pyroxene, plus minor ilmenite, Cr-spinel, and troilite (Fig. A2c). Relatively coarse pyroxene and plagioclase grains have been severely crushed, but not mixed, and they have not been thermally annealed. The largest plagioclase grain in our thin section is equant and about 1 mm across. Plagioclase is relatively uniform in composition, $An_{95.0}$–$An_{96.7}$, but along grain contacts with pyroxene, there are thin, slightly more sodic rims, ranging to $An_{93.6}$ (Table A2). Low-Ca pyroxene is more abundant than augite, and both pyroxenes contain fine lamellar and granular exsolution. Broad-beam analyses of exsolved pyroxenes yield bulk pigeonite (Wo_{16} and $Mg' = 0.54$) and bulk augite (Wo_{31} and $Mg' = 0.59$) compositions (Table A3). A range of crystallization temperatures from 1100 to 1150°C is indicated by the bulk pyroxene compositions (Fig. 3b). The compositions of ilmenite (MgO = 1.2%) and Cr-spinel ($Chr_{66}Ple_{24}Ulv_{10}$) in this sample are similar to those of 67513,7012. Despite measurable siderophile-element concentrations (Table 1), which may be surface contamination, we consider this rock fragment to be essentially monomict.

67513,7052—Ferroan anorthosite

This sample is a 40-mg fragment consisting of 94 vol% plagioclase and ~6% of relatively coarsely exsolved pyroxene, plus traces of olivine and Cr-spinel. Plagioclase grains range in maximum dimension from 0.3 to 1.8 mm and are only moderately fractured. Pyroxene grains range up to 1 mm across and occur interstitial to large plagioclase grains, some having arcuate grain boundaries with plagioclase. The distribution and morphology of pyroxene grains suggest an intercumulus relationship to plagioclase (Fig. A2d).

Plagioclase grains are clouded with 1–5 μm mafic inclusions, oriented in regions where they are fine grained, and irregularly distributed where they coarsen. The inclusions range from elongate, needle-like rods to blebby grains. Plagioclase compositions range from An_{96} to An_{98} and have highly variable Mg/Fe (Table A2), probably resulting from the nonuniform distribution of mafic inclusions and their variable incorporation in broad-beam electron-microprobe analyses. We have not attempted to avoid inclusions in the analyses because we believe the Fe and Mg components to have been dissolved in the original, liquidus plagioclase. The Mg-rich nature, relative to Fe, of some of the individual plagioclase analyses suggest that many of the inclusions may be augite.

Pyroxene consists of inverted pigeonite with augite exsolution lamellae 10–20 μm thick and locally offset or thickened by microfaults. By modal recombination of lamellae of coarse pyroxene, we obtain a bulk pyroxene composition of pigeonite ($Wo_{13.5}$, $Mg' = 0.64$), which suggests a crystallization temperature of about 1125°C (Fig. 3a). Scarce olivine (Fo_{44}) and Cr-spinel ($Chr_{59}Ple_{28}Ulv_{13}$) occur as tiny, interstitial grains and as inclusions in pyroxene.

67513,7061—Ferroan noritic anorthosite

This 27-mg fragment consists of 87 vol% plagioclase and 13% pyroxene, plus trace ilmenite and Cr-spinel (Fig. A2e). It has a strongly cataclastic texture and includes small areas that appear to have been melted and subsequently devitrified. Coarse "clots" of plagioclase grains of nearly uniform extinction preserve a vestige of the former igneous texture. Relict plagioclase grains range up to 0.8 × 1.5 mm and have blocky forms. They are heavily shocked, exhibiting wavy and mosaic extinction, but are not isotropic. Pyroxene grains are typically 0.1 to 0.3 mm in maximum dimension and are of roughly triangular or irregular shapes that occur interstitial to the larger plagioclase grains, suggesting a relict orthocumulus texture, with pyroxene the intercumulus phase. Plagioclase contains abundant, irregularly distributed inclusions of <5 μm across (pyroxene and Fe-Ti-Cr oxides). In our thin section of this sample (Fig. A2e), about a third of the sample looks like finely crushed breccia matrix; this consists of scattered, finely crushed, primary pigeonite and augite in a crushed plagioclase matrix. Exsolution textures and compositions of pyroxene grains confirm that these derive from the same lithology as the coarse-grained parts of the sample.

Plagioclase compositions average An_{96} (Table A2), and exsolved pyroxenes have bulk compositions of pigeonite (Wo_{15}, $Mg' = 0.52$) and subcalcic augite (Wo_{31}, $Mg' = 0.58$) (Table A3). Pyroxene exsolution lamellae range from 5–50 μm thick and their compositions ($Wo_{6.6}$, $Mg' = 0.49$ and Wo_{39}, $Mg' = 0.61$) indicate equilibration at ~800–900°C (Fig. A3b). Cr-spinel ($Chr_{65}Ple_{22}Ulv_{13}$) is compositionally very similar to that of 67513,7012 and ,7097 (Table A4).

67513,7071—Cataclastic ferroan anorthosite

This 25-mg fragment is a strongly fractured, relict single-crystal grain of $An_{96.6}$ plagioclase, about 2 × 3 mm in cross section (Fig. A2f). It contains less than half a percent of scattered, 5–10 μm pyroxene grains (bulk FeO concentration of the sample = 0.20 wt%, Table 1). Low-Ca pyroxene has Mg′ of 0.6 and high-Ca pyroxene, 0.7. Plagioclase is "clouded" with mafic inclusions that are concen-

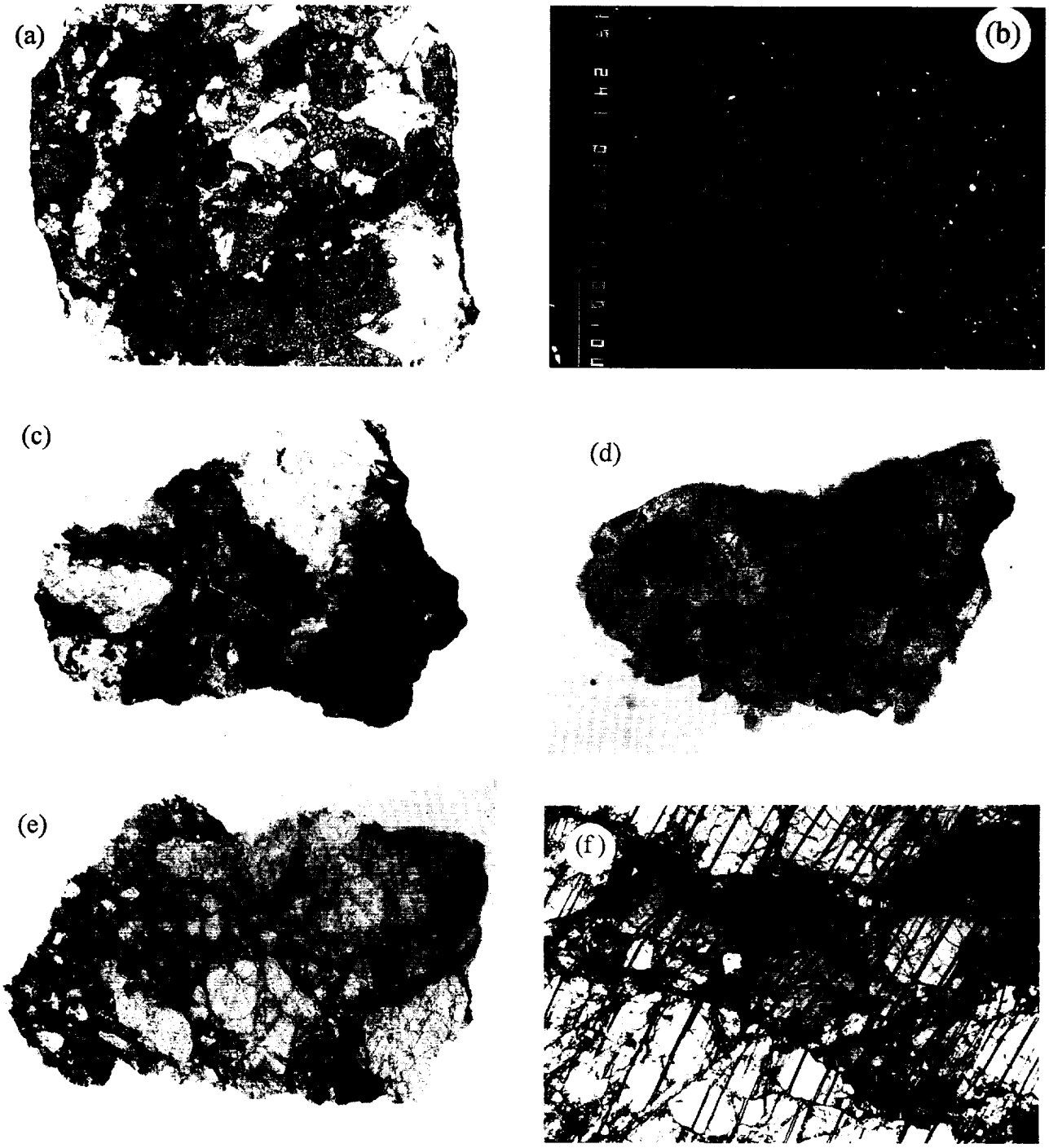

FIG. A2. Photomicrographs showing textures of monomict lithic fragments from sample 67513. (a) Transmitted light photomicrograph of 67513,7012. The right two-thirds show coarse-grained relict texture. In the left-center, running vertically through the section is a crushed zone, but on the basis of mineral compositions, it appears to be the same lithology as the coarse area. Sample is 3 mm across. (b) Backscattered electron image of 67513,7012 composite pyroxene crystal showing early subcalcic augite with thin exsolution lamellae of pigeonite, overgrown by a later generation of pigeonite. Dark regions are plagioclase. Scale bar is 100 μm. (c) Transmitted light photomicrograph of 67513,7097. Sample is 2.8 mm across. Light areas are plagioclase crystals and dark areas are clots of pigeonite and augite. (d) Transmitted light photomicrograph of half of 67513,7052 showing relict igneous texture. Plagioclase in this fragment comprises only two optically continuous grains. Plagioclase is "clouded" with mafic inclusions, but appears slightly clearer along grain boundaries and where the inclusions coarsen (e.g., left-center). Same scale as (c). (e) Transmitted light photomicrograph of 67513,7061. Light areas are shocked single-crystal grains of plagioclase that show only a vestige of relict igneous texture with interstitial pyroxenes. The right side of the section has a cataclastic texture, but similar exsolution textures in pyroxene fragments and uniform compositions of pyroxenes and plagioclase in the coarse-grained and cataclastic regions indicate that the sample is monomict. Sample is 3 mm across. (f) Transmitted light photomicrograph of 67513,7071 with crossed polarizers, showing fractured zone in an approximately 2 × 3 mm single, relict grain of plagioclase. Mafic inclusions, which are readily visible with the polarizers uncrossed, uniformly cloud plagioclase "subgrains," but are concentrated along composition planes of twin lamellae. Field of view is about 1.6 mm.

Table A2. Representative plagioclase compositions in 2–4 mm, ferroan noritic-anorthosite-system lithic fragments from sample 67513, North Ray Crater.

	Monomict samples →												
	,7012 (1)			,7052 (2)				,7061	,7071	,7075			
No. of analyses	avg 20	early 4	late 4	avg 10	high An 2	magn 5	ferr 5	avg 5	avg 4	avg 13	clst A 4	clst B 4	clst C 5
SiO_2	44.60	44.34	45.21	43.90	43.65	44.07	43.73	44.12	44.23	43.47	43.86	43.05	43.37
Al_2O_3	35.49	35.93	35.30	35.77	36.31	35.53	36.00	35.81	35.85	35.94	35.83	36.10	35.74
FeO	0.28	0.29	0.39	0.19	0.29	0.16	0.23	0.13	0.17	0.09	0.07	0.09	0.10
MgO	0.04	0.02	0.03	0.11	0.01	0.21	0.01	0.02	0.12	0.01	0.01	0.01	0.02
CaO	19.20	19.58	18.79	19.85	19.94	19.82	19.87	19.45	19.67	19.80	19.65	19.90	19.71
Na_2O	0.54	0.35	0.70	0.29	0.17	0.32	0.26	0.43	0.38	0.26	0.31	0.20	0.29
K_2O	0.03	0.03	0.04	0.01	0.01	0.02	0.01	0.03	0.01	0.02	0.02	0.02	0.02
Total	100.2	100.5	100.5	100.1	100.4	100.1	100.1	100.0	100.4	99.6	99.7	99.4	99.2
	Cations calculated on the basis of 8 oxygens												
Si	2.058	2.041	2.078	2.031	2.015	2.038	2.024	2.041	2.038	2.021	2.034	2.008	2.024
Al	1.930	1.949	1.912	1.950	1.976	1.937	1.964	1.952	1.947	1.970	1.958	1.984	1.965
Σ Si+Al	3.988	3.990	3.990	3.981	3.991	3.975	3.987	3.993	3.985	3.991	3.992	3.992	3.989
Fe^{2+}	0.011	0.011	0.015	0.008	0.011	0.006	0.009	0.005	0.007	0.004	0.003	0.003	0.004
Mg	0.003	0.001	0.002	0.008	0.001	0.015	0.001	0.002	0.008	0.001	0.001	0.000	0.001
Ca	0.949	0.966	0.925	0.984	0.986	0.982	0.985	0.964	0.971	0.986	0.976	0.994	0.985
Na	0.048	0.031	0.063	0.026	0.015	0.029	0.023	0.039	0.034	0.024	0.028	0.018	0.027
K	0.002	0.002	0.002	0.001	0.000	0.001	0.001	0.002	0.001	0.001	0.001	0.001	0.001
Σ Others	1.014	1.011	1.008	1.026	1.014	1.033	1.019	1.011	1.021	1.015	1.009	1.017	1.019
An	95.0	96.7	93.4	97.3	98.4	97.0	97.6	96.0	96.6	97.6	97.1	98.1	97.2
Ab	4.8	3.1	6.3	2.6	1.5	2.9	2.3	3.9	3.3	2.3	2.8	1.8	2.6
Or	0.2	0.2	0.2	0.1	0.0	0.1	0.1	0.2	0.1	0.1	0.1	0.1	0.1

	Polymict samples →												
	,7097 (1)			,7011				,7024				,7088		
No. of analyses	avg 12	early 3	late 2	avg 22	grain 1 4	grain 2 11	grain 3 7	avg 8	clast 1 2	clast 2 4	clast 3 2	avg 11	clast 1 7	clast 2 3
SiO_2	44.28	44.26	45.23	44.04	44.17	43.97	44.08	44.02	44.31	43.89	44.01	44.20	44.39	43.60
Al_2O_3	35.44	35.61	35.42	35.93	36.19	35.98	35.71	35.73	36.11	35.55	35.73	35.76	35.88	35.90
FeO	0.30	0.15	0.30	0.15	0.06	0.13	0.24	0.52	0.72	0.47	0.41	0.23	0.25	0.21
MgO	0.06	0.06	0.04	0.09	0.01	0.07	0.18	0.05	0.01	0.03	0.16	0.03	0.03	0.03
CaO	19.32	19.32	19.00	19.72	19.75	19.76	19.65	19.44	19.54	19.36	19.50	19.56	19.54	19.63
Na_2O	0.49	0.39	0.67	0.30	0.26	0.32	0.29	0.37	0.31	0.42	0.32	0.44	0.44	0.42
K_2O	0.03	0.03	0.06	0.01	0.01	0.01	0.02	0.02	0.02	0.02	0.01	0.02	0.02	0.02
Total	99.9	99.8	100.7	100.2	100.4	100.2	100.2	100.1	101.0	99.7	100.1	100.2	100.5	99.8
	Cations calculated on the basis of 8 oxygens												
Si	2.051	2.049	2.075	2.033	2.033	2.030	2.037	2.037	2.033	2.039	2.035	2.041	2.043	2.024
Al	1.934	1.943	1.914	1.955	1.963	1.958	1.945	1.948	1.953	1.946	1.948	1.946	1.946	1.964
Σ Si+Al	3.985	3.992	3.989	3.988	3.996	3.989	3.982	3.985	3.986	3.985	3.983	3.987	3.989	3.988
Fe^{2+}	0.012	0.006	0.012	0.006	0.002	0.005	0.009	0.020	0.028	0.018	0.016	0.009	0.010	0.008
Mg	0.004	0.004	0.003	0.006	0.001	0.004	0.012	0.004	0.001	0.002	0.011	0.002	0.002	0.002
Ca	0.959	0.958	0.933	0.975	0.974	0.978	0.973	0.964	0.961	0.964	0.966	0.968	0.964	0.977
Na	0.044	0.035	0.059	0.027	0.023	0.029	0.026	0.033	0.028	0.038	0.029	0.039	0.039	0.038
K	0.002	0.002	0.003	0.001	0.001	0.001	0.001	0.001	0.001	0.001	0.000	0.001	0.001	0.001
Σ Others	1.020	1.005	1.010	1.015	1.001	1.016	1.021	1.021	1.018	1.022	1.023	1.019	1.015	1.026
An	95.5	96.3	93.7	97.3	97.6	97.1	97.3	96.6	97.1	96.2	97.0	96.0	96.0	96.2
Ab	4.3	3.5	5.9	2.7	2.3	2.8	2.6	3.3	2.8	3.7	2.9	3.9	3.9	3.7
Or	0.2	0.2	0.3	0.1	0.1	0.1	0.1	0.1	0.1	0.1	0.0	0.1	0.1	0.1

All Fe assumed to be divalent.

Note (1) For ,7012 and ,7097, "early" plagioclase compositions taken from cores of several coarse grains and "late" compositions from rims or very fine interstitial grains.

Note (2) For ,7052, plagioclase compositions fall into several groups: averages for these are given separately: high An - highest An content; magn - magnesian; ferr - ferroan.

trated preferentially along composition planes of albite twin lamellae. The average FeO and MgO concentrations of plagioclase are 0.17 and 0.12 wt%, respectively (Table A2).

67513,7075—Cataclastic ferroan anorthosite

This 16-mg fragment has a strongly cataclastic texture, with individual, angular plagioclase grains typically <200 μm across. It contains several millimeter-size "clasts" of strongly shocked and slightly annealed plagioclase grains (welded subgrain boundaries, but granoblastic texture not developed) in a very finely crushed, fragmental matrix that is not annealed. Plagioclase compositions range from $An_{97.1}$ to $An_{98.1}$. Pyroxene fragments are very fine grained (<50 μm) and dispersed throughout the crushed plagioclase matrix. Both low-Ca pyroxene (Wo_4, Mg′ = 0.55) and high-Ca pyroxene (Wo_{43}, Mg′ = 0.69) are present. Small (50–100 μm) patches of glassy, presumably shock-melted rock are also scattered throughout the

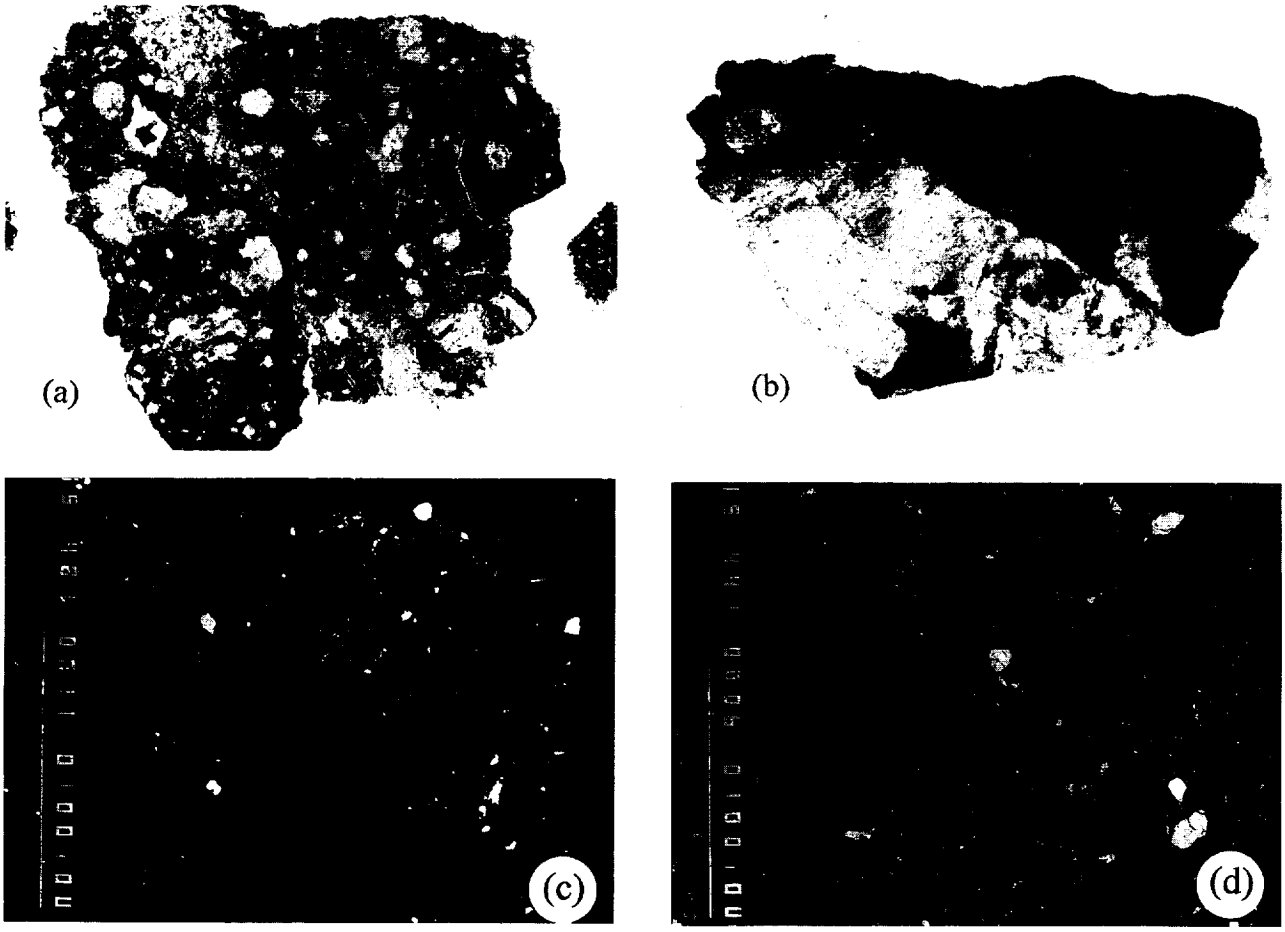

FIG. A3. Photomicrographs of representative polymict lithic fragments from sample 67513. (a) Transmitted light photomicrograph of 67513,7008. Field of view is 3.3 mm. (b) Transmitted light photomicrograph of 67513,7011. Same scale as (a). (c) Backscattered electron image of pyroxene-rich clast in 67513,7024. Vertical scale bar is 100 μm. (d) Backscattered electron image of pyroxene-rich clast in 67513,7088.

fragmental plagioclase matrix. Trace amounts of olivine, Cr-spinel, and ilmenite are present.

Description of Individual Polymict Samples

67513,7008—Fragmental breccia

Sample 67513,7008 is a 32-mg fragmental-matrix breccia containing a seriate distribution of angular to subrounded mineral and lithic clasts that range up to about 1.3 mm across (Fig. A3a). The larger mineral clasts are mostly fragments of single plagioclase grains. Lithic clasts include glassy-matrix melt breccias; angular, glassy impact-melt fragments; granulitic breccias; and fragments of mafic, ferroan igneous rocks. The largest lithic clast in the thin section has a cataclastic texture and an olivine-bearing gabbroic assemblage, similar in appearance to mafic parts of 67513,7061 noritic anorthosite (Fig. A3a, lower left). In this clast, plagioclase compositions are $An_{95.9-96.8}$ and Mg′ of orthopyroxene and augite are 0.58 and 0.70, respectively. Several pyroxene-plagioclase clasts contain fragmented grains up to 400 μm across. Typical mineral compositions are plagioclase An_{96-97} and Mg′ values of low-Ca pyroxene of 0.59. The fine-grained fragmental matrix (not recrystallized) is relatively pyroxene rich and appears to be crushed material similar to the pyroxene-plagioclase lithic clasts. The relatively high bulk Sc concentration of 13.6 ppm reflects the pyroxene-rich nature of this breccia.

67513,7011—Melt-matrix breccia with ferroan anorthosite clast

This 33-mg sample contains a 1 × 1.5 mm clast with a ferroan anorthositic assemblage, half of which is dominated by a single, fractured plagioclase grain (average $An_{97.6}$, Table A2; Fig. A3b). Plagioclase is inclusion rich, similar to that in the monomict lithologies described above, particularly 67513,7052. The clast also contains a 300 μm augite grain (bulk $Wo_{39.5}$, Mg′ = 0.64) and a few scattered, smaller pyroxene grains (Table A3). Small grains of olivine, Fo_{38}, are also present. The large clast is surrounded by a light-brown, glassy matrix containing smaller clasts of the same plagioclase-rich lithology as the large clast. Contacts of the melt matrix with plagioclase clasts are mostly diffuse and indicate partial digestion of plagioclase clasts at the time of melt formation. The melt matrix is glassy to finely crystalline (dark area of Fig. A3b) and has a very feldspathic bulk composition, e.g., Al_2O_3 29–30 wt%. The melt matrix has a normative An content [An/(An + Ab + Or)] of ~0.96 and Mg′ of ~0.5. The major element composition of the impact-melt matrix is essentially the same as that of the bulk lithic fragment (Table 1). Also, the bulk sample has low siderophile element concentrations and a high Sc/Sm value. Thus, we interpret the impact-melt matrix (as well as the clasts) to be dominated by, if not composed exclusively of, the same lithology as the large clast.

67513,7024—Complex breccia

This sample is a 42-mg "complex" melt breccia comprising about 75% clast-bearing melt-matrix breccia with large plagioclase clasts

Table A3. Representative pyroxene compositions in ferroan noritic-anorthosite-system lithic fragments from sample 67513, North Ray Crater.

	Monomict Samples →															
	67513,7012					67513,7052			67513,7061				67513,7071		67513,7075	
	Opx	Aug	InvPig	SubCaAug	Aug	Opx	Aug	bulk Px	Cpx	Opx	Aug	Pig	Opx	Aug	Opx	Aug
	exsolved lamellae		------ bulk analyses -----			exsolved lamellae		recombined	exsolved lamellae		bulk analyses					
SiO_2	51.03	52.18	50.66	50.97	51.44	52.93	52.59	52.84	51.68	51.15	50.41	50.15	52.54	51.37	51.92	52.27
TiO_2	0.19	0.31	0.42	0.52	0.40	0.24	0.46	0.30	0.60	0.25	0.61	0.45	0.25	0.35	0.18	0.38
Al_2O_3	0.39	0.71	0.42	0.66	0.73	0.59	1.08	0.71	1.29	0.48	1.25	0.52	0.76	0.70	0.36	0.79
Cr_2O_3	0.35	0.34	0.32	0.53	0.40	0.28	0.33	0.29	0.35	0.19	0.42	0.25	0.11	0.18	0.13	0.24
FeO	29.20	12.30	25.47	22.07	14.10	23.70	8.86	19.99	14.11	29.06	17.47	25.11	23.80	9.91	26.83	10.98
MnO	0.44	0.23	0.38	0.35	0.26	0.37	0.19	0.33	0.27	0.54	0.32	0.45	0.37	0.18	0.46	0.23
MgO	16.95	12.75	15.98	14.72	13.23	21.29	14.62	19.63	12.31	15.83	13.40	14.96	20.23	13.25	18.42	13.53
CaO	1.09	21.39	5.96	10.23	18.85	0.82	22.20	6.17	19.82	2.44	15.18	6.65	1.64	21.67	1.15	21.49
Na_2O	0.00	0.02	0.01	0.01	0.03	0.01	0.02	0.01	0.02	0.01	0.02	0.02	0.00	0.02	0.00	0.02
Total	99.7	100.2	99.6	100.1	99.4	100.2	100.3	100.3	100.4	100.0	99.1	98.6	99.70	97.64	99.5	99.9
Mg'	0.509	0.649	0.528	0.543	0.626	0.616	0.746	0.636	0.609	0.493	0.578	0.515	0.602	0.704	0.550	0.687
Pyroxene components corrected for Others																
Wo	2.3	42.7	12.1	21.6	37.9	1.7	43.5	13.6	39.4	6.8	30.5	14.7	3.4	44.2	2.4	42.9
En	49.7	37.2	46.4	42.6	38.8	60.5	42.2	55.0	36.9	45.9	40.1	43.9	58.2	39.3	53.7	39.3
Fs	48.0	20.1	41.5	35.8	23.2	37.8	14.3	31.4	23.7	47.3	29.3	41.4	38.4	16.5	43.9	17.9

	Polymict Samples →															
	67513,7097				67513,7011			67513,7024			67513,7088					
	Opx	Aug	Pig	SubCaAug	Opx	Aug	bulk Px	Opx	Aug	bulk Px	Opx	Aug	InvPig	Aug	bulk Pig	bulk Aug
	exsolved lamellae		bulk analyses								Clast 1	Clast 1	Clast 2	Clast 2	Clast 3	Clast 3
SiO_2	51.64	51.81	50.83	50.92	51.74	51.50	51.66	51.45	52.30	51.86	52.00	51.73	52.93	52.22	52.82	51.00
TiO_2	0.16	0.41	0.52	0.82	0.14	0.37	0.37	0.49	0.42	0.49	0.24	0.76	0.33	0.76	0.34	0.94
Al_2O_3	0.39	1.11	0.99	0.83	0.71	3.58	1.60	0.49	0.92	0.85	0.51	1.41	0.54	1.26	0.46	1.56
Cr_2O_3	0.10	0.29	0.36	0.46	0.10	0.26	0.50	0.19	0.21	0.26	0.14	0.30	0.13	0.28	0.23	0.39
FeO	28.77	12.94	23.59	17.05	27.43	12.62	12.83	26.81	11.33	16.21	24.88	10.77	23.63	11.16	22.74	12.85
MnO	0.48	0.23	0.38	0.29	0.40	0.20	0.23	0.44	0.22	0.27	0.44	0.25	0.41	0.21	0.40	0.27
MgO	17.22	12.66	15.57	13.54	18.28	12.29	12.93	18.26	12.76	14.12	18.94	14.17	19.64	14.71	17.61	14.41
CaO	1.34	20.76	7.17	15.35	1.29	19.60	20.30	1.08	21.50	15.50	2.35	20.98	3.30	20.33	5.89	17.49
Na_2O	0.00	0.03	0.01	0.02	0.01	0.11	0.04	0.00	0.03	0.02	0.00	0.00	0.01	0.02	0.00	0.00
Total	100.1	100.2	99.4	99.3	100.1	100.5	100.5	99.2	99.7	99.6	99.5	100.4	100.9	101.0	100.5	98.9
Mg'	0.516	0.636	0.540	0.586	0.543	0.635	0.642	0.548	0.668	0.608	0.576	0.701	0.597	0.701	0.580	0.667
Pyroxene components corrected for Others																
	2.8	41.2	16.6	30.9	2.7	35.9	39.4	2.3	43.0	31.2	4.9	41.4	8.1	40.0	14.3	34.9
	50.2	37.4	45.1	40.5	52.8	40.7	38.9	53.6	38.1	41.9	54.8	41.1	54.9	42.1	49.7	43.4
	47.0	21.4	38.3	28.6	44.5	23.4	21.7	44.1	19.0	27.0	40.3	17.5	37.0	17.9	36.0	21.7

Each analysis represents an average of 2 to 8 electron microprobe spot analyses. All Fe and Mn assumed to be divalent. Pyroxene "others" calculated as in Lindsley and Anderson (1983), except that Al(VI) and Al(IV) reckoned from charge balance requirements assuming the following components: $NaAlSi_2O_6$, $CaCrAlSiO_6$, and $(Fe,Mg)TiAl_2O_6$. For orthopyroxene, the R^{2+} cations of Cr and Al Tschermak's components taken to be Fe and Mg. Excess Ti (>available Al(IV)) assumed to be $(R^{2+})_2TiSiO_6$ where R^{2+}=Ca,Fe,Mg. Abbreviations - Opx: orthopyroxene; Aug: augite; InvPig: inverted pigeonite; SubCaAug: subcalcic augite; Px: pyroxene. "lamellae" indicates that analysis spots were confined to individual lamellae in exsolved pyroxene. "Bulk" indicates that a large spot (30-50 micron diameter) was used to obtain a composite analysis of both low-Ca and high-Ca exsolution lamellae.

and 25% cataclastic anorthositic-gabbronorite breccia. The contact between the two breccia lithologies is diffuse over a thickness of about 100 μm and there is coarsening of the crystalline matrix in this region. It appears that the breccias were welded together while the matrix was still molten.

The anorthositic-gabbronorite breccia has a finely crushed fragmental matrix and contains mineral and lithic clasts ranging up to about 200 μm. The most common lithic clast type is cataclastic gabbronorite comprising exsolved pyroxenes and plagioclase (Fig. A3c). Compositions of coexisting plagioclase (Table A2) and pyroxenes (Table A3) are very similar to those of the igneous, pyroxene-rich lithic fragments such as 67513,7012 and ,7097.

The melt breccia has a brown, glassy to very finely crystalline matrix and about 25% plagioclase clasts that range up to 0.6 mm across. Most clasts are relict single grains of heavily shocked, but not isotropic, plagioclase and have partially resorbed or melted edges. Many of these plagioclase grains are crowded with very fine-grained mafic inclusions, and their typical anorthite content is $\sim An_{97}$.

The matrix of the melt breccia is nearly identical in composition to the bulk sample (e.g., TiO_2, 0.3–0.4; Al_2O_3, 27–29; FeO, 6–6.5; MgO, 3.4–3.7; CaO, 16–17; and Na_2O, 0.36–0.4). That the melt breccia contains mostly anorthite clasts indicates that the anorthositic-gabbronorite fragmental breccia must be at least as mafic in bulk composition, or slightly more so, than the bulk composition of the entire particle. Like the two polymict samples described in the preceding paragraphs, 67513,7024 has low ITE and siderophile-element concentrations (Table 1), the bulk Mg′ is low (0.51), and Sc/Sm is high (20). These characteristics indicate that the components of this complex breccia all derived from a ferroan, relatively mafic (noritic-anorthosite), igneous precursor.

Table A4. Oxide compositions in FNA-system lithic fragments from sample 67513.

	Chrome Spinel					Ilmenite		
Sample	,7012	,7052	,7061	,7097	,7088	,7012	,7097	,7088
SiO_2	0.05	0.05	0.42	0.05	0.03	0.03	0.04	0.02
TiO_2	6.53	5.11	4.78	3.86	3.08	53.1	52.6	52.5
Al_2O_3	9.46	13.47	10.41	11.21	11.95	0.01	0.01	0.03
Cr_2O_3	43.2	43.1	46.1	46.5	48.1	0.23	0.16	0.27
FeO	39.5	36.0	36.1	36.0	34.4	44.9	45.0	45.2
MnO	0.31	0.38	0.38	0.39	0.31	0.49	0.47	0.42
MgO	1.10	1.53	1.05	1.07	1.54	1.32	1.21	1.66
CaO	0.17	0.27	0.69	0.17	0.23	0.07	0.36	0.36
Na_2O	0.02	0.01	0.02	<0.01	0.01	0.00	0.02	0.00
Total	100.3	99.9	99.9	99.3	99.7	100.2	99.9	100.5
Mg'	0.048	0.070	0.049	0.050	0.074	0.050	0.046	0.061
Pleonaste	0.20	0.28	0.22	0.24	0.25			
Chromite	0.62	0.59	0.65	0.66	0.67			
Ulvöspinel	0.18	0.13	0.13	0.10	0.08			

67513,7088—Melt breccia with gabbronorite clasts

This 28-mg sample is also a "complex" breccia in that it contains both melt-matrix breccia, with small, ferroan, mafic clast assemblages and fragmental breccia containing small lithic clasts of the melt-matrix breccia (Fig. A3d). Contacts between the glassy/crystalline-matrix melt breccia and fragmental-matrix breccia are sharp; this, coupled with the occurrence of melt-breccia clasts within the fragmental breccia, indicates that the formation of the fragmental breccia occurred at some time after the melt solidified, but possibly in the same impact event.

The melt-matrix breccia, which is clast-rich and has a glassy to cryptocrystalline matrix, dominates the sample, constituting about 80% of the thin section. Lithic clasts are small, ranging up to only

Table A5. Representative olivine compositions in FNA-system lithic fragments from sample 67513.

Sample No.	,7052	,7008	,7011	,7088	,7088	,7088	,7157	,7157	,7165	,7167
description	avg (3)	avg (2)	clast 1	clast 1	clast 2	clast 3	clast 1	cs R. Ign	vf grain	Lith Cl
SiO_2	34.37	34.36	33.75	33.17	33.31	33.64	34.55	34.51	34.42	34.28
TiO_2	0.02	0.08	0.04	0.03	0.05	0.05	0.02	<0.02	<0.02	0.02
Al_2O_3	0.01	<0.01	<0.01	<0.01	0.01	0.02	0.01	<0.01	<0.01	<0.01
Cr_2O_3	0.04	<0.02	<0.02	<0.02	0.04	<0.02	<0.02	0.03	<0.02	0.02
FeO	44.71	44.25	49.20	48.02	46.26	46.87	41.35	45.14	44.81	45.53
MnO	0.49	0.51	0.54	0.53	0.47	0.48	0.42	0.46	0.55	0.49
MgO	19.68	20.28	16.76	17.27	20.25	18.30	23.46	20.70	19.91	20.29
CaO	0.22	0.17	0.20	0.09	0.13	0.17	0.06	0.10	0.10	0.08
Na_2O	<0.01	<0.01	<0.01	<0.01	<0.01	<0.01	<0.01	<0.01	<0.01	<0.01
Total	99.5	99.7	100.5	99.1	100.5	99.5	99.9	100.9	99.8	100.7
	*	*	*	*	*	*			*	
Mg'	0.44	0.45	0.38	0.39	0.44	0.41	0.50	0.45	0.44	0.44
Fa	55.8	54.9	62.0	60.9	56.1	58.8	49.7	54.9	55.7	55.7
Fo	43.8	44.8	37.7	39.0	43.7	40.9	50.2	44.9	44.1	44.2

All Fe assumed to be Fe^{2+}. (*) Analyses of grains < 100 microns across, therefore CaO concentrations may be high due to fluorescence from adjacent plagioclase or augite. Sample 67513,7157 is a composite fragment containing feldspathic glassy-matrix melt breccia welded to a relatively coarse-grained olivine-gabbroic-anorthosite lithology that has relict igneous texture. Although this sample is not described in the text, its olivine composition is included here because coarse olivine is rare among the ferroan mafic lithologies in 67513. Clast 1 occurs in the melt breccia, and those designated as coarse, relict igneous (cs R. Ign) and very fine grained (vf-grain) coexist with plagioclase (An 96.7), orthopyroxene (Mg' 0.58), and clinopyroxene (Mg' 0.66) in the olivine-gabbroic-anorthosite lithology. Olivine in this lithology is not mantled by orthopyroxene. Olivine in 67513,7165 occurs as mafic granules within a coarse plagioclase grain (An 96.7), coexisting with orthopyroxene (Mg' 0.56), in a monomict ferroan-anorthositic breccia. Olivine in 67513,7167 occurs as ~100 μm grains in a lithic clast with plagioclase (An 96.8) and pigeonite (Mg' 0.58).

several hundred microns, and many comprise only a few grains having relict igneous contacts. Lithic-clast assemblages in this sample (similar to those in ,7008) are unusual compared to most other mafic lithic fragments from 67513 in that they contain appreciable olivine in addition to plagioclase and exsolved pyroxene. Pyroxene and olivine grains are highly ferroan (Tables A3 and A5) and ilmenite and Cr-spinel are common and compositionally similar to those in 67513,7012 and ,7097 (Table A4).

The bulk composition of 67513,7088 (Table A1) is ferroan ($Mg' = 0.53$) and is among the most mafic of the polymict samples (FeO > 8% and Sc ~ 16 ppm). The composition of the melt-breccia matrix is very similar to the bulk composition of the sample, suggesting that the precursor of both melt and clasts was the same lithology, distributed widely enough (laterally or vertically) to form melt in one region that was then mixed with unmelted clasts of the same rock elsewhere.